Atmos. Chem. Phys. Discuss., 13, 17953–18005, 2013
www.atmos-chem-phys-discuss.net/13/17953/2013/
doi:10.5194/acpd-13-17953-2013

Atmospheric Chemistry and Physics Discussions

Strong wintertime ozone events in the Upper Green River Basin, Wyoming

B. Rappenglück[1], L. Ackermann[1], S. Alvarez[1], J. Golovko[1], M. Buhr[2], R. Field[3], J. Soltis[3], D. C. Montague[3], B. Hauze[4], S. Adamson[4], D. Risch[4], G. Wilkerson[4], D. Bush[5], T. Stoeckenius[6], and C. Keslar[7]

[1]Department of Earth and Atmospheric Sciences, University of Houston, Houston, Texas, USA
[2]Air Quality Design, Boulder, CO, USA
[3]University of Wyoming, Laramie, WY, USA
[4]Meteorological Solutions Inc., Salt Lake City, UT, USA
[5]T&B Systems, Santa Rosa, CA, USA
[6]Environ, Novato, CA, USA
[7]Wyoming Department of Environmental Quality, Cheyenne, WY, USA

Received: 29 May 2013 – Accepted: 27 June 2013 – Published: 5 July 2013

Correspondence to: B. Rappenglück (brappenglueck@uh.edu)

Published by Copernicus Publications on behalf of the European Geosciences Union.

Abstract

During recent years, elevated ozone (O_3) values have been observed repeatedly in the Upper Green River Basin (UGRB), Wyoming during wintertime. This paper presents an analysis of high ozone days in late winter 2011 (1 h average up to 166 ppbv). Intensive Operational Periods (IOPs) of ambient monitoring were performed which included comprehensive surface and boundary layer measurements. On IOP days, maximum O_3 values are restricted to a very shallow surface layer. Low wind speeds in combination with low mixing layer heights (~ 50 m a.g.l. around noontime) are essential for accumulation of pollutants within the UGRB. Air masses contain substantial amounts of reactive nitrogen (NO_x) and non-methane hydrocarbons (NMHC) emitted from fossil fuel exploration activities in the Pinedale Anticline. On IOP days in the morning hours in particular, reactive nitrogen (up to 69 %), aromatics and alkanes (~ 10–15 %; mostly ethane and propane) are major contributors to the hydroxyl (OH) reactivity. Measurements at the Boulder monitoring site during these time periods under SW wind flow conditions show the lowest NMHC/NO_x ratios (~ 50), reflecting a relatively low NMHC mixture, and a change from a NO_x-limited regime towards a NMHC limited regime as indicated by photochemical indicators, e.g. O_3/NO_y, O_3/NO_z, and O_3/HNO_3 and the EOR (Extent of Reaction). OH production on IOP days is mainly due to nitrous acid (HONO). Until noon on IOP days, HONO photolysis contributes between 74–98 % of the entire OH-production. Ozone photolysis (contributing 2–24 %) is second to HONO photolysis. However, both reach about the same magnitude in the early afternoon (close to 50 %). Photolysis of formaldehyde (HCHO) is not important (2–7 %). High HONO levels (maximum hourly median on IOP days: 1096 pptv) are favored by a combination of shallow boundary layer conditions and enhanced photolysis rates due to the high albedo of the snow surface. HONO is most likely formed through (i) abundant nitric acid (HNO_3) produced in atmospheric oxidation of NO_x, deposited onto the snow surface and undergoing photo-enhanced heterogeneous conversion to HONO (estimated HONO production: 2250 pptv h^{-1}) and (ii) combustion related emission of

ACPD
13, 17953–18005, 2013

HONO (estimated HONO production: ~ 585 pptv h^{-1}). HONO, serves as the most important precursor for OH, strongly enhanced due to the high albedo of the snow cover (HONO photolysis rate 2900 pptv h^{-1}). OH radicals will oxidize NMHCs, mostly aromatics (toluene, xylenes) and alkanes (ethane, propane), eventually leading to an increase in ozone.

1 Introduction

The Upper Green River Basin (UGRB) has one of the largest natural gas reserves of the United States (US). In 2009, the proven gas reserves for the Jonah field (11.1 billion cubic meters) ranked seventh and for the Pinedale Anticline field (13.8 billion cubic meters) ranked third among the top 100 natural gas fields in the US (EIA, 2009). Oil and Gas extraction including drill rigs, production equipment and compressor stations are operating continuously and represent the only significant emission source in the UGRB with overall emissions of 9.9 metric tons/day of reactive nitrogen (NO_x) and 41.7 metric tons/day of volatile organic compounds (VOC) (WDEQ, 2011).

The UGRB is a high plateau located about 2000 m a.s.l.. It is surrounded by mountain ranges which reach heights up to 3500 m a.s.l. to the West (Wyoming Peak) and 4200 m a.s.l. to the Northeast (Gannett Peak). Winters are usually cold and frequently associated with snow cover. During recent years, elevated hourly ozone values above 150 ppbv have been observed in the UGRB during wintertime (Schnell et al., 2009; Carter and Seinfeld, 2012). As of July 2012, the US Environmental Protection Agency (EPA) declared the UGRB as a non-attainment area for the 2008 ground-level 8 h ozone standard, which is 75 ppbv. Recent publications have focused on some observational findings in the UGRB in the year 2008 (Schnell et al., 2009) or sensitivity analysis using a box model approach together with VOC (Volatile Organic Compound) incremental reactivities for selected ozone episodes in 2008 and 2011 (Carter and Seinfeld, 2012). Still, there are major uncertainties in our understanding of the occurrence of high ozone levels in the UGRB under wintertime conditions. Apart from specific mete-

ACPD
13, 17953–18005, 2013

orological conditions for the UGRB (i.e. low mixing layer heights, light winds, extensive snow cover, at times recirculation of air masses), these include processes in the nitrogen oxide (NO_x) and VOC cycles, such as the role of nitric acid (HNO_3) and the radical precursors such as formaldehyde (HCHO) and nitrous acid (HONO). In particular, high daytime HONO levels were found (Rappenglück, 2010, 2011). Although HCHO levels were moderate, the sources and role of HCHO in the UGRB is not fully understood, particularly with regard to the overall relatively low alkene reactivity as shown by Carter and Seinfeld (2012). A better quantification of these hydroxyl (OH) sources is needed to improve the description of ozone chemistry in the UGRB, which is required to develop efficient strategies to reduce pollution in that area.

In this paper we analyze high ozone days in late winter 2011 (1 h average up to 166 ppbv) observed in the area of the Boulder station and describe the meteorological and chemical processes leading to these extreme events using the comprehensive surface and boundary layer measurements collected during the Upper Green Winter Ozone Study (UGWOS) 2011 (MSI, 2011).

2 Methods

Surface air quality data used in this paper were collected continuously at the Boulder site and Boulder South Road site from January–March 2011 (for Boulder South Road site data see also Field et al., 2011). Boundary layer measurements including radiosonde and ozonesonde launches were performed at the Boulder site during Intensive Operational Periods (IOPs). Data from the tethered balloon were obtained at the "Tethered Balloon" site. Table S1 lists the details of the instrumentation and Fig. 1 shows the location of these sites in the UGRB including the locations of oil and gas wells.

Surface measurements included routine measurements for ozone (O_3), reactive nitrogen compounds ($NO/NO_2/NO_x$), total non-methane hydrocarbon (NMHC), methane (CH_4) and trace level measurements for nitrogen monoxide (NO), nitrogen dioxide

ACPD
13, 17953–18005, 2013

(NO_2), and total reactive nitrogen (NO_y). Additional measurements included nitric acid (HNO_3), nitrous acid (HONO), formaldehyde (HCHO), carbon monoxide (CO) and on-line speciated NMHC. If not otherwise indicated the term NMHC denotes total, i.e. non-speciated NMHC measured at the Boulder or "Tethered Balloon" site. A specific measurement design was applied for the HONO measurements. The sampling unit for the HONO measurements was attached to a small tower. The sampling unit stayed at the surface (10 cm above the ground) for 15 min, then moved to the top of the tower (1.80 m above the ground), where it stayed for another 15 min, afterwards the unit returned back to the surface and resumed a new cycle. Upward and downward motions lasted 2 min and were accomplished by a step motor. The purpose was to explore whether HONO gradients close to the surface could be detected. Note: for comparison of HONO data with any ancillary chemistry and meteorological data obtained in this study, HONO data collected at 1.80 m above the surface was used.

At all sites, basic meteorological measurements were made. Additional details beyond the information provided in Table S1 can be found in MSI (2011).

3 Results and discussion

3.1 General observations

The Upper Green River Basin had continuous snow cover throughout the winter months January–March 2011. Figure 2 shows that ambient temperature was below freezing most of time, ranging from −28.0 °C in early February to +5.1 °C in mid-March. Also displayed in the same figure are ambient ozone observations. A slight increase in background ozone from 45 ppbv in January to about 50 ppbv in March is discernible. Apart from this longer term variation, it can clearly be seen that at times significant day-to-day variations in the ozone mixing ratios may occur. While decreases of ozone are reflecting NO titration effects, strong increases of ozone well above the ozone background level are likely due to a combination of dynamic and photochemical processes. During

ACPD
13, 17953–18005, 2013

the time frames 28 February–2 March and 9–12 March 2011, the highest hourly ozone readings were observed with up to 166 ppbv at the Boulder surface site on 2 March. IOPs were performed during these two periods (IOP#1: 28 February–2 March; IOP#2: 9–12 March), which included additional information about the vertical distribution of meteorological parameters as well as some selected trace gases. The following discussions will focus on the time period 28 February–16 March 2011. This time period includes the two IOPs and has the most complete data availability with regard to continuous as well as discrete measurements. The non-IOP days during this time frame will be used as reference days.

Figure 3a, b display mean diurnal variations of O_3, NO, NO_x, NMHC, CH_4, NO_y, HNO_3, HONO, and HCHO split into IOP and non-IOP days. Most species show 2–3 times higher mixing ratios on IOP days compared with non-IOP days throughout the day. Ozone shows this enhancement during the afternoon and early evening only. Primarily emitted species like NO show maximum values during the time frame 09:00–12:00 MST (Mountain Standard Time). Species which also can be formed secondarily (e.g. NO_y, HNO_3, HONO, and HCHO) exhibit enhanced levels during sunlit daytime hours from about 07:00–18:00 MST, in particular on IOP days. Ozone mixing ratios start to increase by 09:00 MST, reach maximum levels around 15:00 MST and remain at higher levels until early evening. Quite surprisingly, HONO mixing ratios are high during the daytime on non-IOP days and even higher on IOP days (maximum median around noontime 1096 pptv) which, compared to other locations, is quite unusual (see e.g. Stutz et al., 2010a). Conventional thinking suggests that HONO levels would instead decrease due to both photolysis and to increased mixing in the boundary layer during the day. The median HONO levels on IOP days are similar to those observed at a highly frequented Houston highway junction (Rappenglück et al., 2013).

A statistical summary for IOP and non-IOP days is given in Table S2. In the following discussion, we refer to median values. It shows that in the morning hours (05:00–09:00 MST), the median mixing ratios of most species are enhanced by a factor of 2 on IOP days vs non-IOP days. Some are almost unchanged (e.g. HNO_3, NO_y, ozone).

ACPD
13, 17953–18005, 2013

During photochemically active daytime periods (11:00–17:00 MST), the median of most compounds is enhanced by 50–100 %, HCHO is enhanced by 171 % and HONO by as much as 278 %, which hints to significant secondary daytime formation of these species. During the nighttime period, NO_x (mostly composed of NO_2) and HNO_3 show the highest enhancements on IOP days (121 % and 138 %, respectively). HONO and HCHO are also enhanced (98 % and 64 %, respectively). Overall, on IOP days trace gases relevant to O_3 formation are all significantly enhanced throughout the day compared with non-IOP days.

The only major anthropogenic emissions in the remotely located UGRB are associated with oil and gas extraction. As a benchmark for this study we compare some results to a highly polluted urban area. Luke et al. (2010) report results of reactive nitrogen compounds for Houston, Texas, a city exposed to complex emissions including emissons from large petrochemical sources (e.g. Parrish et al., 2009; Lefer and Rappenglück, 2010; Olaguer et al., 2013). An investigation of the same daytime periods shows that, while NO_x is significantly higher in the urban air of Houston (about 2–4 times higher when compared to IOP days at Boulder), the picture is different for NO_y. Although NO_y is higher in Houston in the morning and during the night (275 % and 186 %, respectively), it is lower in Houston than in Boulder during daytime on IOP days. These differences are largely due to HONO and HNO_3. While HONO is slightly lower in the morning and during the night, it is about three times higher during the daytime on IOP days. HNO_3 on the other hand is higher throughout the day on IOP days in Boulder compared to the Houston case. On non-IOP days at Boulder, HONO and HNO_3 levels are mostly lower than in Houston. The HNO_3 fraction of NO_y is around 18 % during daytime on non-IOP days, while it is around 22 % during daytime on IOP days (Luke et al., 2010, report an overall daytime HNO_3 fraction of 15.7 % of NO_y in Houston). For HONO the corresponding numbers are around 2 % (non-IOP days) and 4.5 % (IOP days), while Luke et al. report an overall daytime HONO fraction of 1.7 % of NO_y.

ACPD
13, 17953–18005, 2013

Luke et al. (2010) also report temporally highly resolved data for particulate nitrate NO_3^- (p-NO_3^-). Median values were 0.234 ppbv (05:00–09:00 CST), 0.091 (11:00–17:00 CST), and 0.135 ppbv for nighttime (21:00–05:00 CST). At Boulder, 24 h samples were collected. Although not exactly comparable, it may provide us with some estimate. On IOP days, the median value for p-NO_3^- was equivalent to 0.58 ppbv (maximum equivalent to 1.54 ppbv), while on non-IOP days the corresponding values were equivalent to 0.47 ppbv and 0.74 ppbv, respectively, which indicates that p-NO_3^- may be higher at the Boulder site than in Houston.

Figure S3 shows a comparison of NO_y measurements versus individual NO_y compounds for the Boulder site. Particulate data was only collected on a 24 h basis. Therefore this data set only comprises a small number of observations. The deviation from the 1 : 1 line is within the accuracy of the NO_y and the combined individual NO_y measurements (see Table S1) for ranges above 20 ppbv. For NO_y values below 20 ppbv, NO_y tends to be larger than the sum of the individually measured NO_y components. According to Fig. S3, still some fraction of NO_y compounds may be missing, even when particulate NO_3 was included. Potential candidates for this NO_y deficit include the nitrate radical (NO_3), dinitrogen pentoxide (N_2O_5), nitrylchloride ($ClNO_2$), peroxy acetylnitrate (PAN) and alkyl nitrates. While NO_3, N_2O_5, and $ClNO_2$ would be present at nighttime (e.g. McLaren et al., 2004; Edwards et al., 2013), PAN and alkyl nitrates are produced photochemically and tend to reach maximum values during daytime (e.g. Hayden et al., 2003; Sommariva et al., 2008 and references therein). No measurements of these species were performed at the Boulder site, however some assumptions can be made. Maximum NO_3 and N_2O_5 levels typically range from about 50 pptv and 300 pptv, respectively, in polluted continental air masses (McLaren et al., 2004) to about 150 pptv and 500 pptv, respectively, in urban areas (Stutz et al., 2010b). NO_3 and N_2O_5 can constitute 7–30 % of NO_y (McLaren et al., 2004 and references therein). NO_3 is formed through the reaction of NO_2 with O_3. It is likely that this reaction may be efficient at the Boulder site due to the observed appreciable ambient levels of NO_2 and O_3 (see Table S2 and Fig. 2). Loss mechanisms for NO_3 include reactions with

ACPD
13, 17953–18005, 2013

alkenes and biogenic hydrocarbons, and reaction with NO_2 to form N_2O_5. As alkenes and biogenic hydrocarbons are found at low levels in the UGRB (Field et al., 2012a,b), the latter reaction to form N_2O_5 is likely the dominant removal process for NO_3. The homogeneous and heterogeneous hydrolysis of N_2O_5 may ultimately lead to appreciable amounts of gaseous HNO_3 and particulate nitrate according to McLaren et al. (2004). While no direct measurements of $ClNO_2$ were performed at the Boulder site, particulate chloride (Cl^-) data show low median levels of 0.015 µg m^{-3} (based on 6 24 h filter samples). This may indicate that Cl^- is not abundantly available to form $ClNO_2$ in appreciable amounts, likely less than 600–800 pptv found in the Uintah Basin in Utah (Edwards et al., 2013). Earlier studies in the UGRB also included PAN measurements (MSI, 2009). The results showed up to 1 ppbv PAN during daytime and up to 400 pptv as an estimated 24 h average. As high PAN values would also coincide with high NO_y values, we assume that PAN would only account for a negligible amount of around 1 % percent of the NO_y budget based on the results shown in Fig. S3. Alkyl nitrates may account for about 10 % of NO_y (Sommariva et al., 2008 and references therein). As alkyl nitrates have an atmospheric lifetime of more than a week they may accumulate under favorable meteorological conditions and contribute to the NO_y budget not only during the day, but also at night. We predominantly found lower values for NO_y at night (see Fig. 3b), i.e. at a time when the missing NO_y components NO_3, N_2O_5, $ClNO_2$, and also alkyl nitrates would contribute most to the NO_y budget. This may explain the deficit found in the NO_y budget at NO_y mixing ratios below 20 ppbv.

Corresponding analysis for NO_x oxidation products NO_z ($NO_z = NO_y - NO_x$) versus the sum of individual NO_z compounds $NO_{z,i}$, i.e. HNO_3, HONO and p-NO_3^- based on a 24 h data base yielded NO_z [ppbv] = $\Sigma NO_{z,i}$ [ppbv] · 1.09 – 0.38 ppbv (r^2 = 0.87) for IOP days and NO_z [ppbv] = $\Sigma NO_{z,i}$ [ppbv] · 1.12 + 0.28 ppbv (r^2 = 0.82) for non-IOP days, which is of similar magnitude as found in Houston (Luke et al., 2010), for instance. Luke et al. point out that higher nighttime $NO_z/NO_{z,i}$ ratios and the magnitude of $NO_z - NO_{z,i}$ differences may point to the presence of nighttime $ClNO_2$. Based on our limited data we cannot make similar statements, but cannot rule out this possibility. Our

ACPD
13, 17953–18005, 2013

measurements did not include PAN. Using our previous assumptions of about 400 pptv as an estimated 24 h average value, PAN could contribute up to 5 % of the NO_z budget. The atmospheric lifetime of PAN (τ_{pan}) is primarily determined by the following reactions:

$$CH_3C(O)OONO_2 \rightarrow CH_3C(O)OO + NO_2 \quad (1)$$

$$CH_3C(O)OO + NO_2 \rightarrow CH_3C(O)OONO_2 \quad (2)$$

$$CH_3C(O)OO + NO \rightarrow CH_3C(O)O + NO_2 \quad (3)$$

The atmospheric lifetime of PAN thus critically depends on the NO_2/NO ratio and also the ambient temperature, since reaction constant k_1 is proportional to $\exp(-1/T)$. Based on Reactions (1)–(3), τ_{pan} can be calculated according to Ridley et al. (1990):

$$\tau_{PAN} = \frac{1}{k_1}\left(1 + \frac{k_2[NO_2]}{k_3[NO]}\right) \quad (4)$$

For the Boulder site, the shortest τ_{pan} for IOP#1 was 10.6 days and for IOP#2 2.6 days and reached almost 1 day on the last day of the field study (16 March) when temperature reached +5.1 °C. It is thus unlikely that PAN may serve as a NO_2 source and contribute to ozone formation under the environmental conditions found during the study. However, it can serve as a NO_x reservoir and remove NO_x out of the UGRB.

3.2 Role of meteorological parameters

3.2.1 Dependence on wind direction

Figure S4a, b display daytime and nighttime wind roses of O_3, primarily emitted pollutants NO_x, NMHC, CH_4, and trace gases that may have both primary and secondary sources, i.e. NO_y, HNO_3, HONO, and HCHO. Figure S4a, b include both IOP and non-IOP days in order to obtain larger and more representative data sets. Regardless of

ACPD
13, 17953–18005, 2013

IOP and non-IOP days, night-time data will most likely be useful to point to potential emission sources as photochemical processes are at a minimum.

The daytime ozone wind rose clearly shows enhanced mixing ratios for SSW to WSW and SE/ESE directions (median 64–73 ppbv). During nighttime, maximum median ozone of about 60 ppbv occurs under NNE–ENE wind directions. These wind directions only have small amounts of NO_2 (median about 1.5 ppbv; not shown) and are likely more aged air masses. Primarily emitted NO_x, NMHC, and CH_4 display pronounced enhancements during the daytime in the similar directions as for O_3. During nighttime there are significant peaks under SW–W wind directions. While NO_x and NMHC are distinctly enhanced ($NO_x \sim 10$ ppbv, NMHC ~ 900 pptv), still CH_4 with about 4 ppm is a factor of 2 above its background levels. This hints to sources which emit nitrogen oxides, NMHC and CH_4 or different sources located in the same area which may overlap. This is likely consistent with locations of compressors and drill rigs operating during January–March 2011 (which emit primarily NO_x) relative to well head production equipment (which emits primarily CH_4 and NMHC).

NO_y, HNO_3, HONO, and HCHO (Fig. S4b) largely follow the same directional pattern as NO_x and hydrocarbons (Fig. S4a). However, contrary to the primarily emitted pollutants NO_x, NMHC, and CH_4, species also formed secondarily, i.e. HNO_3, HONO, and HCHO generally show higher values during daytimes. This indicates their dual nature, i.e. primarily emitted (as reflected in the nighttime data) and, in addition, secondarily formed (as seen in the daytime data). NO_y behaves somewhat similarily to the primary pollutants, most likely due to the large fraction of NO_x in NO_y (see Table S2). Interestingly, HONO clearly shows an anisotropic dependence on wind direction, both during night- and daytime, which indicates a point source rather than an area source like the surface. During daytime, HONO mixing ratios are highest from WSW to SSW (median 477 pptv to 545 pptv, respectively), while at night maximum mixing ratios occur under WSW wind direction (median 347 pptv). While the nighttime HONO peak for WSW flow is in accordance with those for other trace gases and hints at a point source, the high daytime HONO levels (see also Table S2) are at odds with the conventional

ACPD
13, 17953–18005, 2013

understanding of HONO diurnal variability, suggesting that additional processes other than point source emissions (e.g. Czader et al., 2012 and references therein) may be important.

3.2.2 Backward trajectories

For further analysis, we calculated HYSPLIT (HYbrid Single-Particle Lagrangian Integrated Trajectory) backward trajectories (Draxler and Hess, 2013; Rolph, 2013) based on 12 km resolution meteorological data provided by NAM (North American Mesoscale model). Uncertainties stated by Draxler and Hess are in the range of 15–30 % of the travel distance. As an additional test, we calculated back and forward trajectories within the UGRB for the times of interest and found only negligible difference among those. Although, there might be some limitations associated with the accuracy of backward trajectories, they at least may provide information about major regimes. The results of trajectory calculations are shown in Fig. 4 and they indicate three major regimes during the 28 February–16 March 2011 period. Non-IOP days mostly showed consistent air mass flows out of the NW wind sector (example shown 8 March 2011). Also, they are associated with higher wind speeds and enhanced atmospheric dispersion. This coincides with the generally low to modest levels of pollutants (Fig. S4a, b). The days with the highest ozone levels during each IOP may show recirculation processes during the day (as for 3 March 2011); however, they are usually characterized by the fact that at least once during the day, trajectories eventually pass through the area Southwest of Boulder before arriving at Boulder. According to Fig. 1, air masses would then pass the oil and gas well locations of the Pinedale Anticline and also a large number of compressor facilities (Fig. 5). According to the trajectories on 12 March, air masses would have passed this sector at the most 1–2 h before arrival at Boulder and would have stayed in that region for about 1 h. As seen in Fig. S4a, b, air masses coming from the SW quadrant carry maximum amounts of both primary and secondary pollutants. As shown later, they are also associated with the highest VOC reactivity and a change of NO_x sensitivity towards a VOC sensitivity regime.

ACPD
13, 17953–18005, 2013

3.2.3 Boundary layer height

Tethersonde data taken on IOP days indicate very shallow boundary layer heights. Based on the data in Fig. S5 and using approaches by Stull (1988), average morning boundary layer heights (09:00–11:00 MST) would be estimated to be about 35 m a.g.l. around noon (11:00–13:00 MST), around 50 m a.g.l. in the early afternoon (13:00–15:00 MST), reach a daily maximum around 80 m a.g.l., and in the late afternoon (15:00–17:00 MST) decrease to around 45 m a.g.l. This is largely in agreement with SODAR data (not shown). Figure 6 shows vertical profiles of ozone and wind direction on IOP days. Generally, IOP days were characterized by W to NW flows above 600 m a.g.l. and appreciable temporal and spatial changes in wind direction below this level. These lower level changes are also reflected in the backward trajectories previously shown in Fig. 4. Below 600 m a.g.l., windspeed was generally less than 5 m s^{-1}. Above 600 m a.g.l., wind speed rapidly increased above 10 m s^{-1} (not shown). The strong changes in atmospheric flow around 600 m a.g.l. certainly helps to maintain inversions and stable boundary layer conditions beneath this layer throughout IOP days. Since surrounding mountain ranges of the UGRB reach heights up to 3500 m a.s.l. to the West (Wyoming Peak) and 4200 m a.s.l. to the Northeast (Gannett Peak), the boundary layer air masses are easily trapped within the basin and recirculation processes as shown for 2 March in Fig. 4 are likely. This is in accordance with earlier wintertime meteorological studies in similar areas of the Rocky Mountains (Yu and Pielke, 1986).

Figure 6 shows that ozone exhibits a distinct behaviour associated with the atmospheric dynamic pattern: above 600 m a.g.l., ozone mixing levels are quite stable around 60 ppbv regardless of the day and time of the day. It represents background ozone levels in the well mixed lower troposphere. Below 600 m a.g.l., ozone mixing ratios clearly show diurnal changes with lower than background values in the early morning and strongly enhanced values in the afternoon. The maximum deviations are clearly restricted to a very shallow surface layer. There is no evidence of ozone carry over from

ACPD
13, 17953–18005, 2013

previous days. Ozone deposition over dry surfaces is about 0.4 cm s^{-1} (Hauglustaine et al., 1994); however, it is about 0.07 cm s^{-1} over snow surfaces (Hauglustaine et al., 1994), i.e. ozone removal through turbulent diffusion is significantly reduced. Recent studies over polar snow indicate even lower deposition velocities in the range of 0.01–0.07 cm s^{-1} (Helmig et al., 2009). As deposition may play a minor role during snow covered periods in the UGRB, the ozone deviation from the background ozone level is instead determined by removal (e.g. nighttime titration) and daytime in-situ formation processes.

As an example, Fig. 7 shows selected data obtained by the tethersonde system for the IOP day 2 March 2011. The results for ΔT (Delta-T in the plot) indicate well defined inversion and stable conditions in levels with $\Delta T > 0\,^{\circ}$C. Again, it can be seen that highest ozone levels are restricted to the surface levels. Precursors such as NO_2 and NHMC may exhibit a layered distribution. Highest levels may occur close to the mixing layer height as defined by ΔT. This hints to pollution plumes which may have originated from either elevated sources and/or sources which show some plume rise due to higher than ambient temperatures. Potential ozone O_x, as expressed by the sum of O_3 and NO_2 provides information about the potential presence of O_3 formation processes. Using the tethersonde data and segregating it into time frames like in Fig. S5, we obtain Fig. S6. This figure shows two main features: (i) formation of O_3 from early morning to the afternoon throughout the surface layer and (ii) apart from the late afternoon, a tendency towards higher O_x values in higher layers of the surface layers. Highest O_x mixing ratios at the surface occur only in the late afternoon.

In an attempt to investigate other trace gases for which no vertically resolved data is available, we segregated surface data into 5 m bins of hourly SODAR mixing layer height (MLH) data and split it into day- and nighttime observations. Results are shown in Fig. S7. For ozone, daytime data is clearly higher than nighttime data regardless of the MLH. However, during daytime, maximum ozone levels are observed under lowest MLH. Speciated NMHC data obtained at the Boulder South Road site generally show enhanced values under MLH < 40 m a.g.l. and decreasing concentrations with increas-

ACPD
13, 17953–18005, 2013

ing MLHs regardless of the time of day. However, while higher nighttime concentrations of speciated NMHC classes are found at lower MLHs, during daytime, the lowest MLHs are associated with lower concentrations of NMHC classes. Assuming NMHC sources which do not change emission strength during the day, this points to photochemical degradation of NMHCs in the lowermost surface layers. The change in the median values is about −20 % for alkanes, −45 % for alkenes, and almost −50 % for aromatics. CO does not change significantly with MLH and time of day. NO_x shows significantly higher values during daytime and, contrary to NMHC classes, there is no change at lowermost MLHs when comparing daytime with nighttime observations. However, nighttime data clearly shows decreasing NO_x levels with increasing MLHs. Both HCHO and HONO show higher values during the daytime than nighttime regardless of MLHs. In accordance with other primary pollutants like NMHC and NO_x, HCHO and HONO exhibit a trend towards lower mixing ratios with increasing MLHs during nighttime.

In general, results from IOP days, such as 2 and 12 March, indicate that slightly variable wind directions (including reciruclation) and low wind speeds in combination with low boundary layer heights are essential for accumulation of both primary and secondary pollutants. The occurrence of low boundary layer heights in presence of snow cover in mountainous regions is in accordance with previous model simulations (Bader and McKee, 1985). These studies also showed that these conditions can hold a stable layer until very late in the day.

3.2.4 HONO and relationships with radiation and relative humidity

Some photo-enhanced heterogeneous reactions are currently being discussed as likely daytime HONO sources (Kleffmann, 2007). Figure S8 shows a comparison of HONO data obtained close to the surface (10 cm above the surface) and at about 1.80 m above the surface. It reflects the main results of Fig. 3b with higher HONO levels during the daytime. However, two additional observations are evident: (i) scatter in the HONO data is greater at the 1.80 m level, where maximum concentrations are found in the morning and early afternoon. The absence of these early morning high levels in the surface data

ACPD
13, 17953–18005, 2013

suggest that the observed maximum at 1.80 m may be due to transport of HONO rather than a surface source. (ii) The median HONO values at the surface show a significant increase around noon coinciding with the strongest solar irradiation, and surpass those at the 1.80 m level. This suggests a strong surface source of HONO which is most efficient around noontime. According to Villena et al. (2011), HONO photolysis can be the most important OH radical source in polar regions under clean conditions (e.g. in polar regions), in particular when HONO was not correlated to CO and NO_x, which would otherwise hint to direct emissions. From Figs. S8 and S4b, it is evident that daytime photochemical processes contribute to HONO formation at the Boulder site, while transport is important throughout the day. Potential direct combustion related emissions will be discussed later.

As pointed out by Stutz et al. (2004), relative humidity may be favorable for HONO formation, at least in urban environments. Figure S9 shows that on IOP and non-IOP days, HONO levels are higher during the day than at night, regardless whether the measurements were taken close to the surface or at 1.80 m a.g.l. During nighttime, photochemical processes are at a minimum. A trend towards higher HONO levels with increasing higher relative humidity can be discerned, with a maximum around 80 %. Again, this does not seem to depend on the measurement height. A dependency of the $HONO/NO_2$ ratio on relative humidity as described by Stutz et al. (2004) could not be identified in our data set, likely due to the fact that the snow cover itself provided a constant amount of water, which would be in line with observations by Wojtal et al. (2011) for aqueous surfaces.

3.3 Role of emissions and chemistry

3.3.1 Potential combustion emissions for radical precursors HCHO and HONO

Primary sources for HCHO and HONO are important sources for the hydroxyl radical (e.g. Ren et al., 2013; Czader et al., 2013). While HCHO may have a variety of primary sources, its secondary formation during daytime usually exceeds primary HCHO

ACPD
13, 17953–18005, 2013

emissions significantly (e.g. Rappenglück et al., 2010 and references therein). This is also reflected in the Boulder site data when comparing daytime HCHO data on IOP vs. non-IOP days (see Table S2 and Fig. 3b). Also secondarily produced HCHO may be a source for new radicals.

Unfortunately, there were no CO measurements taken at the Boulder site, but linear regression analysis of CO versus NO_x calculated for the Boulder South Road site indicate CO [ppbv] = 6.14 × NO_x [ppbv] + 140 [ppbv] (r^2 = 0.55) over all wind directions for the entire time period 28 February–16 March 2011. The slope is very close to values obtained for urban traffic rush hour, which is $6.01 \pm 0.15\,\mathrm{ppbv\,CO\,(ppbv\,NO_x)^{-1}}$ (Rappenglück et al., 2013). While the correlation coefficient is significantly weaker than found in the Rappenglück et al. (2013) study (r^2 = 0.91), which may be due to higher degree of mixing of different air masses, it indicates the presence of combustion sources; under remote unpolluted conditions CO and NO_x would be almost unrelated (see e.g. Villena et al., 2011).

As previously mentioned, compressors and drill rigs were operating during January–March 2011 in the area located upwind of the Boulder site under SW flow conditions. These units emit primarily NO_x relative to well head production equipment which primarily emits CH_4 and NMHC. As indicated in Fig. S4a, b, enhanced levels of primary pollutants occur under SSW–W flows during daytimes and under SW–W flows during the night. In an attempt to identify potential emission sources for HCHO and HONO, we performed correlation analyses with various other trace gases measured at the Boulder site focussing on nighttime data, to exclude daytime photochemical processes and SW–W wind directions which showed peak values for all species in accordance with Fig. S4a, b. NO_z/NO_y ratios were around 0.35 under these wind flow conditions and thus, significantly less than 0.6, indicating freshly emitted pollutants.

Table S10 clearly shows the close relationship between HONO and NO_2, NO_x, and HNO_3 as observed at the Boulder site. The good, although somewhat weaker, correlation of HONO with total NMHC at the Boulder site is most likely due to the fact that emission sources which emit NO_x may be located close to NMHC sources. HCHO

ACPD
13, 17953–18005, 2013

shows overall weaker correlations with NO_x, total NMHC, and CH_4 compared with HONO. HCHO has a longer atmospheric lifetime than HONO and thus some appreciable background, which may also include remnants of previous day formation of HCHO. This background may get mixed into freshly emitted plumes and cause higher data scatter. In any case, according to Table S10, HCHO shows stronger correlation with total NMHC and CH_4 than with NO_x, while for HONO it is the opposite behaviour. This hints to different source categories for HONO and HCHO.

Based on the CO/NO_x observations at the Boulder South Road, we assume that NO_x at the Boulder site would also be primarily related to combustion sources. In a recent traffic related emission study, measurements of HONO versus NO_x yielded a slope of 15.86 ± 0.82 pptv HONO (ppbv $NO_x)^{-1}$ ($r^2 = 0.75$) and a slope of 25.00 ± 1.06 pptv HCHO (ppbv $NO_x)^{-1}$ ($r^2 = 0.80$) for HCHO versus NO_x (Rappenglück et al., 2013). The slopes of HONO versus NO_x for the Boulder nighttime data under wind direction 180°–270° and the Houston traffic related measurements are almost identical. In the traffic emissions study, Rappenglück et al. argued that the high $HONO/NO_x$ emission ratios were likely due to heavy duty vehicles. In the case of the Upper Green River Basin, stationary diesel powered compressors may act similarly. For HCHO versus NO_x, the slopes are significantly lower than found in traffic related combustion emissions. The correlation coefficient is also weaker. It is likely that different emission sources overlap. Since HCHO shows a closer correlation with total NMHC at the Boulder site and even closer with CH_4 as shown in Table S10, it is likely that well head equipment, in addition to co-located compressors, may contribute to HCHO emissions. Interestingly, contrary to HCHO, HONO displays a stronger correlation with total NMHC than with CH_4. This may further support the ideas that HONO emissions are more related to combustion (compressors) and HCHO has some overlapping emissions originating from drill rig operations.

ACPD
13, 17953–18005, 2013

3.4 NMHC versus NO_x limitation of ozone production

Observation based methods like photochemical indicators such as O_3/NO_y, O_3/NO_z, and O_3/HNO_3 and the EOR (Extent of Reaction) can be used to evaluate whether ozone production at a given location may be VOC or NO_x limited (Sillman, 2002; Sillman and He, 2002). The EOR is defined as:

$$EOR = \left(1 - \frac{NO_x}{1.3 \cdot NO_y}\right)^{0.67} \quad (5)$$

Table S11 lists ranges of indicator values which are representative of different regimes. We calculated the photochemical indicators for the Boulder site. For this analysis, we focus on the IOP days, as those were the days with maximum ozone levels. It is common to all photochemical indicators that they display significant changes throughout the day depending on the wind direction (Fig. 8). Generally, median values of all indicators would point towards NO_x limitation of ozone production, which would be expected for rural areas. However, in most cases during morning hours (07:00–11:00 MST) and/or under SW flow conditions, all indicators reach minimum values. Table S12 shows that O_3/NO_y and the EOR would indicate VOC limitation; the values of the other indicator values would fall into the transitional regime according to Table S11. On non-IOP days, the values for the photochemical indicators would be slightly higher but still show a similar diurnal and wind directional pattern. Change from a NO_x-limited regime towards a VOC limited regime implies reaching or passing the transitional regime, where ozone production can be most efficient and can reach maximum values as shown by Mao et al. (2010). The periods with the lowest values for photochemical indicators generally coincide with minimum values of the $NMHC/NO_x$ ratio as observed at the Boulder site (Fig. 9). This minimum value is about 50 and represents a relatively high value compared to urban areas (Mao et al., 2010). This could be due to relatively low NMHC reactivity, either caused by low temperatures or a NMHC mixture which is mostly com-

ACPD
13, 17953–18005, 2013

posed of slow reacting hydrocarbons (e.g. alkanes such as ethane and propane), or a combination of both.

3.5 OH reactivity

In order to describe the importance of individual or classes of trace gases with regard to photochemical processes, it is important to consider both the reactivity and the amount of these trace gases in ambient air. One way to do this is to calculate the propene equivalent J as proposed by Chameides et al. (1992):

$$J = C_J \frac{k_{OH}(J)}{k_{OH}(C_3H_6)} \quad (6)$$

with C_J being the mixing ratio of hydrocarbon compound J in ppbC or any other compound J in ppbv, the reaction rate of this compound with OH (k_{OH}) and normalized to the reaction rate of propene with OH ($k_{OH}(C_3H_6)$). This approach expresses any individual or classes of trace gases in terms of propene units. However, it is an approximation as reactions other than with OH, i.e. with O_3, NO_3, and Cl, are neglected. In our approach, we merge data from the Boulder South Road site (speciated NMHC, CH_4, CO, NO_x) with data collected at the Boulder site (HCHO, HONO) to have a most comprehensive data set. During the winters of 2011 and 2012 nineteen canister surveys of speciated NMHC were performed at sites throughout the UGRB. Boulder and Boulder South Road are located three miles from each other. The Boulder site is closer to the spine of the Pinedale Anticline development and concentrations at this site are generally slightly higher than Boulder South Road. While the r^2 for the comparison of data from these two sites for each of four surveys during February and March 2011 were each greater than 0.97, there is some variation of slope between the two sites with values ranging from 1.2 to 1.7. The two Boulder sites share the characteristic of measuring air that is influenced by a wide range of oil and gas emission sources (Field et al., 2012a,b) with similar contributions between NMHC classes. When considering speciated NMHC alkanes are most correlated and aromatic are least correlated. Although

ACPD
13, 17953–18005, 2013

there might be slight differences in the atmospheric chemistry settings of both sites, we believe that this will not have major impacts on the general findings. Figure 10 displays the diurnal variation of the fractions of the propene-equivalent on IOP days. Within the speciated NMHC obtained at the Boulder South Road site, the most important contributions to the overall OH reactivity stem from aromatics (50–60 %), alkanes (30–40 %) and the remaining ~ 10 % alkenes. As expected, the contribution from alkynes and isoprene is negligible due to their low reactivity (alkynes) and low mixing ratios (isoprene). Although CH_4 accounts for the largest fraction of all hydrocarbons (ranging from 90 % around noon to 95 % in the moning hours on a ppb basis), its propene-equivalent fraction is quite modest with 1–2 % due its low reactivity. This pattern does not change much throughout the day and is not much different on non-IOP days (not shown). It should be noted that in terms of absolute propene-equivalents, OH-reactivity on IOP days reaches up to 48 ppbC before noon compared to 31 ppbC around the same time on non-IOP days. While alkanes contribute to the propene-equivalent about twice as much on IOP days than on non-IOP days, the contribution by aromatics increases by about 30 %, whereas the contribution by alkenes stays about the same. When other compounds are included (CO, NO_x, HCHO, HONO), it becomes apparent that NO_x plays an important role both in terms of contribution to reactivity as well as to the diurnal change of contributions. On IOP days aromatics contribute about 35–40 %, alkanes 20–30 %, NO_x 20–40 %, and alkenes about 5–10 % to the overall propene-equivalent. The remaining ~ 5 % are due to CO, HONO, HCHO, alkynes, and CH_4. The contribution from NO_x reaches its maximum from 05:00–09:00 MST. The picture is different on non-IOP days, where NO_x contributions are significantly lower throughout the day. More specifically, the contributions to the propene-equivalent on non-IOP days would be: aromatics 40–60 %, alkanes, 20–40 %, NO_x 10–35 %, alkenes 5–10 %, and ~ 5 % for the remaining trace gases CO, HONO, HCHO, alkynes, and CH_4.

ACPD
13, 17953–18005, 2013

Figure 11 displays OH reactivity based on the sum of the reaction rate coefficients multiplied by the mixing ratios of reactants with OH (Mao et al., 2010):

$$k_{OH} = \sum k_{OH+VOC_i}[VOC_i] + k_{OH+CO}[CO] + k_{OH+NO}[NO] + k_{OH+NO_2}[NO_2] + k_{OH+HNO_3}[HNO_3] + \ldots \quad (7)$$

Figure 11 clearly shows that on IOP days OH reactivity is higher than on non-IOP days by a factor of 2. On IOP days, the magnitude of OH reactivity is comparable to that found in direct OH measurements for urban air in Houston, Texas (Mao et al., 2010). Contrary to the urban Houston case, where NO_x may contribute up to 50 % to OH reactivity during the rush hour, for the Boulder case NO_x may contribute up to 69 % throughout the day. This may be due to NO_x emission sources in the Boulder area whose emissions strength does not change much throughout the day (e.g. compressors). Another distinction is that, at Boulder, alkenes may contribute around 5 % to the overall OH reactivity while for the Houston case, it can be up to 35 %. The contribution from alkanes is in the 10–15 % range at Boulder, while in Houston it is about 5–10 %. The contribution of aromatics is about the same for both cases (10–15 %).

In accordance with Fig. S4a, b, also the absolute propene-equivalent displays similar distribution with highest values under SW wind directions. The reactivity mix does not change that much with wind direction (i.e. mostly aromatics, alkanes, and NO_x), mostly from SW. Figure 12 shows that while alkanes contribute 80–85 %, aromatics around 10–15 %, and alkenes less than ~ 5 % of NMHCs on a mass basis, aromatics contribute 50 % and alkanes around 45 % to the propene-equivalent as observed at the Boulder South Road site. Still, contributions by alkenes are low. Contributions from CH_4 and isoprene are negligible.

The major finding is that on IOP days in the morning hours in particular, NO_x (and to some extent HONO as it is closely associated with NO_x), aromatics and alkanes (the latter ones largely dominated by ethane and propane) are major contributors to the OH reactivity and propene equivalent at Boulder. Highest reactivities are found in air masses arriving at the Boulder site under SW flow conditions. This time period and

ACPD
13, 17953–18005, 2013

wind flow condition largely coincide with the lowest NMHC/NO_x ratios observed at the Boulder site and a switch from NO_x limited to transitional, if not VOC limited regime, with the largest ozone production efficiency as described in the previous Sect. 3.4. Under VOC limited conditions, it is likely that highly reactive aromatics, such as toluene and xylenes, may be most efficiently competing with other NMHCs in reactions with OH. NO_x reactions with OH in turn will cause substantial formation of HNO_3.

3.6 Role of HONO

As discussed, major removal processes for OH at the Boulder site involve reactions with NO_x, aromatics, and alkanes. Sources for OH are photolysis processes of O_3, aldehydes (foremost HCHO), H_2O_2, $ClNO_2$, and HONO. Nighttime alkene ozonolysis may also contribute to OH formation. Recent studies suggest that major OH formation occurs through HONO photolysis in the morning, HCHO photolysis in late morning, and O_3 photolysis throughout the day, whereas photolysis of H_2O_2 and alkene ozonolysis are of minor importance during the day (Elshorbany et al., 2009; Ren et al., 2013; Czader et al., 2013). According to an analysis by Elshorbany et al. (2009), HONO photolysis can contribute to about 52 % of radicals on a 24 h average, followed by alkene ozonolysis (about 20 %), HCHO photolysis (about 15 %) and ozone photolysis (about 4 %) in an urban area. On the other hand, in unpolluted polar regions HONO is suggested to be a major radical source (98 %) and ozone photolysis would account for the remaining 2 % (Villena et al., 2011). Mao et al. (2010) report that contributions to the radical pool from HONO photolysis may be highest in high NO_x environments. For the Boulder site, we suspect that nighttime alkene ozonolysis is negligible. Median values for ethene and propene are about 25 % and 7 % of those found in urban areas like Houston (Leuchner and Rappenglück, 2010) and thus may play an even lower role than in Houston where it was found to be of least importance (Ren et al., 2013). As mentioned earlier we presume that $ClNO_2$ may not be present in appreciable amounts based on the low levels of particulate chloride. However, ozone and HONO (see also Table S2) at the Boulder site can exceed values found in urban areas.

ACPD
13, 17953–18005, 2013

Figure 13 displays results of calculation of OH-production due to photolysis of ozone, HCHO, and HONO for IOP and non-IOP days. Median data for ozone, HCHO, and HONO were taken. While a surface albedo of 80 % for snow cover was considered, the data do not take into account the altitude of the Boulder site (2000 m a.s.l.). Thus OH-production may actually be even higher than shown in the plots. Nevertheless, the results clearly indicate that OH production on IOP days is mainly due to HONO. Until noon, HONO photolysis contributes between 74–98 % of the entire OH-production. Ozone photolysis (2–24 %) is second to HONO photolysis. However, both reach about the same magnitude in the early afternoon (close to 50 %). The picture is different on non-IOP days, where HONO surpasses the OH-contribution by ozone photolysis in the early morning hours only. The absolute contribution to OH-production caused by ozone photolysis and HCHO photolysis on IOP days does not differ much from non-IOP days. In both cases the photolysis of HCHO contributes mostly less than 10 % (on IOP days 2–7 %) to the overall OH-production and is thus not important. It is worth noting that the calculated OH-production due to HCHO photolysis represents an upper limit as we did not distinguish between primary and secondary HCHO in these calculations. These results are different from the simulation analyses for a site in the Uintah Basin, Utah (Edwards et al., 2013). Potential reasons may include that Edwards et al. assumed a uniform increase of O_3 precursors by a factor of 2 under cold pool events, that the site may have been exposed to a different ambient chemical matrix (e.g. HCHO is significantly higher, while HONO is significantly lower at the Horse Pool site, UT, compared to the Boulder site, WY) and that they assumed a primary fraction of 50 % of the observed daily integrated HCHO mixing ratio.

For the Boulder site, it is the photolysis of HONO, which makes a significant difference from non-IOP days to IOP days, as it is 6 times higher on IOP days. The high OH-production rate of 2900 pptv h^{-1} by HONO-photolysis must be balanced by HONO sources of the same magnitude.

At the Boulder site no speciated photolysis rates measurements were available. As a surrogate, we plotted measured incoming ultraviolet (UV) radiation in Fig. 14. On IOP

ACPD
13, 17953–18005, 2013

days, incoming UV radiation was on the order of 10 % higher than on non-IOP days. Data in Fig. 14 shows that HONO increases as incoming UV radiation increases. The $HONO/NO_x$ ratio is about the same value for IOP and non-IOP days throughout the nighttime. In particular, in the morning hours from 05:00–09:00 MST, when maximum levels of primary pollutants are present (Fig. 3a), the $HONO/NO_x$ ratio tends to be at a minimum and is between 2–5 % in both cases, which is similar to other locations. However, it increases significantly from 12:00–14:00 MST on non-IOP days (median values ∼ 10 %) and from 11:00–16:00 on IOP days (median values up to 30 %). During the same time periods, nitrogen oxide levels decrease (Fig. 3a). This indicates that more HONO is being formed through NO_2 conversion. Also during the same time periods, O_3 increases as well. It appears likely that HONO is being produced through photo-enhanced formation processes which are most efficient when snow cover is present.

It has become evident that ambient HONO concentrations are higher than can be accounted for by direct emissions and that heterogeneous processes on surfaces may lead to enhanced ambient HONO levels. In particular, these processes tend to occur on surfaces with adsorbed water in the dark (Finlayson- Pitts et al., 2003; Jenkin et al., 1988; Kleffmann et al., 1998) based on the following reaction (Goodman et al., 1999; Kleffmann et al., 1998):

$$NO_{2(ads)} + H_2O_{(ads)} \rightarrow HONO_{(ads)} + HNO_{3(ads)} \quad (8)$$

Recently, an additional nighttime formation of HONO that was not related to NO_2 was reported on aqueous surfaces in the marine boundary layer by Wojtal et al. (2011), assuming a surface nano layer saturated with NO_2 precursors and no irreversible loss of HONO from that layer. Wojtal et al. observed that $HONO/NO_2$ ratios would increase during the night from 3–30 % and even higher on some occasions, with HONO levels about 1 ppbv at night. While we suspect that the snow surface could have been saturated with NO_2 precursors due to appreciable amounts of these compounds in ambient air (see Fig. 3a, b), we did not observe increasing $HONO/NO_x$ ratios throughout the

ACPD
13, 17953–18005, 2013

night as shown in Fig. 14. Also, HONO mixing ratios were 3–10 times lower compared to the Wojtal et al. study.

Over the last decade a variety of photo-enhanced HONO formation mechanisms have been discussed to explain observations of elevated daytime HONO levels (Kleffmann, 2007). These include: (i) the photolysis of surface adsorbed nitrate or nitric acid (Zhou et al., 2001, 2002; Ramazan et al., 2006), (ii) the photolysis of ortho-nitrophenols (Bejan et al., 2006), (iii) light-induced NO_2 reduction on surface adsorbed humic acid films (Stemmler et al., 2007), (iv) gas-phase reaction of electronically excited NO_2, due to photolysis, with water (Li et al., 2008), and (v) the conversion of HNO_3 to HONO on primary organic aerosol (Ziemba et al., 2010).

As mentioned in Sect. 3.1, observations at the Boulder site were characterized by remarkably high ambient levels of HONO, HNO_3, and p-NO_3^- which on IOP days were higher than in urban air measurements, e.g. in Houston, Texas. HONO showed close correlation with HNO_3 not only during nighttimes (S10) but, contrary to NO_2 and NO_x, also during daytime regardless of IOP or non-IOP days with correlation coefficients ranging from 0.73 and 0.80. Contrary to Ziemba et al. (2010), who found that HONO was anticorrelated with HNO_3 during morning traffic rush hours, our observations do not show any anticorrelation during any time period. We thus assume that conversion of HNO_3 to HONO on primary organic aerosol will be negligible in the UGRB. HNO_3 on IOP days formed a higher fraction of NO_y than in Houston (22 % vs 16 %). Its fraction of NO_z ranged between 30–40 %, with maximum values found under SW wind directions. Again, corresponding values in Houston were only about 20 % (Luke et al., 2010). Particulate NO_3^- at the Boulder site was closely related to EC, elemental carbon, (r^2 = 0.85) and OC, organic carbon (r^2 = 0.73), but only showed poor correlation with sulfur (r^2 = 0.09) and sulfate r^2 = 0.03). This fingerprint is likely associated with fossil fuel combustion in industrial processes (Jacobson, 2012). Björkman et al. (2013) studied dry deposition velocities for HNO_3 and p-NO_3^- onto snow surfaces in the arctic. They found that the dry deposition velocity for particulate NO_3^- critically depends on the particle size; still, for particle sizes around 7 µm, the dry deposition velocity is

ACPD
13, 17953–18005, 2013

significantly lower than for HNO_3. Overall, the dry deposition of p-NO_3^- only accounts for 1–7 % of the total nitrate dry deposition (Björkman et al., 2013). According to Reaction (8) $HNO_{3(ads)}$ can already be formed through $NO_{2(ads)}$. Dry deposition velocity of HNO_3 onto snow surfaces is about 50 times greater than for NO_2 (Hauglustaine et al., 1994). Using median data for NO_2 and HNO_3 mixing ratios as shown in Table S2 dry deposition flux of HNO_3 onto the snow surface may be about 8–65 times greater than for NO_2, with maximum values during daytime, as HNO_3 mixing ratios surpass those of NO_2. While Reaction (8) would likely contribute to HONO formation throughout the day as shown by Wojtal et al. (2011) over aqueous surfaces, we assume that deposition of HNO_3 would be of critical importance, in accordance with studies by Zhou et al. (2003).

When adsorbed on a surface, the following reactions may occur (Mack and Bolton, 1999; Zhou et al., 2002, 2003):

$$HNO_{3(ads)} + h\nu \rightarrow [HNO_3]^*_{(ads)} \quad (9)$$

$$[HNO_3]^*_{(ads)} \rightarrow HNO_{2(ads)} + O(^3P)_{(ads)} \quad (10)$$

$$[HNO_3]^*_{(ads)} \rightarrow NO_{2(ads)} + OH_{(ads)} \quad (11)$$

Reaction (9) requires sunlit daytime conditions. $NO_{2(ads)}$ formed in reaction (11) may then further react according to Reaction (8) and subsequently form HONO. According to Zhou et al. (2003), the production yield of HONO from surface HNO_3 photolysis is almost independent of relative humidity between 20–80 %, although some moisture is necessary. Thus snow cover would provide a favorable substrate. On the other hand, the negligible dependence on relative humidity may explain, at least partly, why we did not find a clear correlation of HONO with relative humidity.

Zhou et al. (2003) calculate HONO formation rates based on surface HNO_3 photolysis. We adopted this approach to explore whether this process may balance the median HONO photolysis rate of 2900 pptv h^{-1} at the Boulder site around noontime on IOP days. According to Zhou et al. the upward flux F_{up} of NO_x and HONO can be

ACPD
13, 17953–18005, 2013

described as follows:

$$F_{up} = \alpha \cdot J \cdot v \cdot C \cdot t \quad (12)$$

where α represents the fraction of the average of the individual median values for the diurnal variation of the UV radiation (Fig. 14) versus the noontime maximum value of the UV radiation. This value is about 25 % and is used to determine the fraction of deposited HNO_3 exposed to noontime photolysis rate J_{HNO_3} (s^{-1}). The parameter v is the average HNO_3 dry deposition velocity, C is the ambient HNO_3 concentration ($mol\,m^{-3}$) and t (s) is the accumulation time since the last precipitation. Zhou et al. applied the following values for their calculation: $J_{HNO_3} = 2.5 \times 10^{-5}\,s^{-1}$, $v = 2 \times 10^{-2}\,m\,s^{-1}$, $C = 700\,pptv = 3.1 \times 10^{-8}\,mol\,m^{-3}$, and $t = 24\,h = 86.400\,s$. For the estimate at the Boulder site, we consider a different HNO_3 concentration and also assume a different photolysis rate J_{HNO_3} due to higher albedo. The median HNO_3 mixing ratio on IOP days at Boulder was 2.1 ppbv (which equals $9.37 \times 10^{-8}\,mol\,m^{-3}$). According to Finlayson-Pitts and Pitts (2000) and references therein, photolysis rates for ozone, HCHO, and HONO, which we used to calculate OH-production, are about 2.5 times higher over surfaces with 80 % albedo (e.g. over snow) compared with standard surfaces. We assume the same magnitude of change for J_{HNO_3}. Zhou et al. calculated a HONO production rate of $\sim 150\,pptv\,h^{-1}$ for a 100 m boundary layer height. The specific conditions for the Boulder site would lead to ~ 7.5 times higher HONO emission than found in the Zhou et al. study, i.e. $1125\,pptv\,h^{-1}$. Boundary layer measurements at Boulder were around 50 m a.g.l. around noontime on IOP days, which would result in a HONO emission flux of $2250\,pptv\,h^{-1}$. Apart from surface emissions combustion related HONO emissions may contribute to the HONO flux. As outlined earlier we found a robust $HONO/NO_x$ emission ratio of $15\,pptv\,HONO\,(ppbv\,NO_x)^{-1}$ during nighttimes under SW flow conditions. In the quadrant southwest of Boulder multiple facilities related to oil drill activities are distributed over an area of $\sim 300\,km^2$. According to the WDEQ inventory (WDEQ, 2011) the overall NO_x emission from these facilities is $\sim 1180\,kg\,h^{-1}$ with about 91 %

ACPD
13, 17953–18005, 2013

originating from drill rig and completion emissions. The overall NO_x flux in this area would be $\sim 4000\,\mu g\,m^{-2}\,h^{-1}$. Assuming a boundary height of 50 m a.g.l. this would result in an increase of $\sim 39\,ppbv\,h^{-1}$ for NO_x and an increase of $\sim 585\,pptv\,h^{-1}$ for HONO using the emission ratio of 15 pptv HONO (ppbv NO_x)$^{-1}$. We assume that these emissions may be transported to the Boulder site and that removal processes may be negligible. Both the surface HONO flux due to photolysis of HNO_3 adsorbed on the snow surface and the combustion related HONO emissions would account for a total HONO production rate of $2835\,pptv\,h^{-1}$ at around noontime on IOP days, which is in very good agreement with the photolysis rate of HONO of $2900\,pptv\,h^{-1}$. We therefore conclude that ultimately, NO_x emitted into the extremely shallow boundary layer during the wintertime season in the UGRB is causing high HONO levels. This occurs from two processes: (i) HNO_3 produced during atmospheric oxidation of NO_x, can be deposited onto the snow surfaces which facilitate subsequent photo-enhanced heterogeneous conversion to HONO and (ii) through combustion related emission of HONO. HONO, in turn, will serve as the most important precursor for OH, strongly enhanced due to the high albedo of the snow cover. The high altitude of the UGRB (2000 m a.s.l.), which we did not consider in our calculations, may likely intensify these processes.

4 Conclusions

During the periods 28 February–2 March and 9–12 March 2011, designated Intensive Operational Periods (IOPs), high hourly ozone readings up to 166 ppbv were observed at the Boulder surface site, located in the Upper Green River Basin, Wyoming. These values were well above the estimated surface background ozone of ~ 40 ppbv and lower tropospheric ozone background of ~ 60 ppbv in March. Intensive During the IOPs comprehensive surface measurements were performed and observations of vertical distributions of meteorological parameters and selected trace gases were carried out. The observed high ozone levels likely result from a combination of multiple factors.

ACPD
13, 17953–18005, 2013

Maximum ozone values are restricted to a very shallow surface layer. There is no evidence of ozone carry over from previous days. Ozone levels may remain stable as ozone deposition velocity onto snow surfaces is low. On IOP days, slightly variable wind directions (including reciruclation) and low wind speeds in combination with low mixing layer heights (~ 50 m a.g.l. around noontime) are essential for accumulation of both primary and secondary pollutants within the UGRB. IOP days are usually characterized by the fact that, at least once during the day, trajectories eventually pass through the area Southwest of Boulder before arriving at the Boulder site. Recirculation processes within the basin may also occur. Air masses would then pass the oil and gas well locations of the Pinedale Anticline and also a large number of compressor facilities at the most 1–2 h before arrival at Boulder and would have stayed in that region for about 1 h. Compressors and drill rigs emit primarily NO_x, relative to well head production equipment, which emits primarily CH_4 and NMHC. While compressors and drill rigs would also emit HONO and to some extent HCHO, well head production equipment would only contribute to emissions of HCHO. This is largely supported in an analysis of nighttime ratios of HONO and HCHO versus NO_x, NMHC, and CH_4 in air masses coming from this area. In general, these air masses contain maximum amounts of both primary and secondary pollutants. They are also associated with the highest VOC reactivity and a change of NO_x sensitivity towards a VOC sensitivity regime.

On IOP days in the morning hours in particular, NO_x (up to 69 %), then aromatics and alkanes (~ 10–15 %; mostly ethane and propane) are major contributors to the OH reactivity and propene equivalent at Boulder. Highest OH reactivities (up to 22 s^{-1}) are found in air masses arriving at the Boulder site under SW flow conditions. This time frame (and also wind direction) largely coincides with the lowest NMHC/NO_x ratios at the Boulder site and a change from a NO_x-limited regime towards a VOC limited regime, which implies reaching or passing the transitional regime where ozone production can be most efficient and can reach maximum values. This is supported by photochemical indicators such as O_3/NO_y, O_3/NO_z, and O_3/HNO_3 and the EOR (Extent of Reaction). The NMHC/NO_x at the Boulder site during these periods is ~ 50

ACPD
13, 17953–18005, 2013

and represents a relatively high value compared to urban areas. This could be due to relatively low NMHC reactivity, either caused by low temperatures or a NMHC mixture which is mostly composed of slow reacting hydrocarbons (e.g. alkanes), or a combination of both. Under VOC limited conditions, it is likely that highly reactive aromatics, such as toluene and xylenes, may be most efficiently competing with other NMHCs in reactions with OH. NO_x reactions with OH in turn will cause substantial formation of HNO_3.

OH production on IOP days is mainly due to HONO. Until noon HONO photolysis contributes between 74–98 % of the entire OH-production. Ozone photolysis (2–24 %) is second to HONO photolysis. However, both reach about the same magnitude in the early afternoon (close to 50 %). On non-IOP days, HONO surpasses the OH-contribution by ozone photolysis only in the early morning hours. The absolute contribution to OH-production caused by ozone photolysis and HCHO photolysis on IOP days does not differ much from non-IOP days. In both cases the photolysis of HCHO contributes mostly less than 10 % (on IOP days 2–7 %) to the overall OH-production and is thus not important.

We conclude that ultimately, NO_x emitted into the extremely shallow boundary layer during the wintertime season in the UGRB is causing high HONO levels (maximum hourly median on IOP days: 1096 pptv) through (i) HNO_3 produced in atmospheric oxidation of NO_x, deposited onto the snow surface and undergoing photo-enhanced heterogeneous conversion to HONO (estimated HONO production: 2250 pptv h^{-1}) and (ii) combustion related emission of HONO (estimated HONO production: $\sim$ 585 pptv h^{-1}). HONO, in turn, serves as the most important precursor for OH, strongly enhanced due to the high albedo of the snow cover (HONO photolysis rate 2900 pptv h^{-1}). OH radicals oxidize NMHCs, mostly aromatics (toluene, xylenes) and alkanes (ethane, propane), eventually leading to an increase in ozone. The data does not suggest that relative humidity favors the presence of high levels of HONO. This may be due to the assumptions that the surface HNO_3 photolysis is almost independent of relative humidity (Zhou et al., 2003) or the limitation of our data, which always showed relative humidity well

ACPD
13, 17953–18005, 2013

above 50 % during nighttimes. The high altitude of the UGRB (2000 m a.s.l.), which we did not consider in our calculations, may likely intensify these processes.

Supplementary material related to this article is available online at: http://www.atmos-chem-phys-discuss.net/13/17953/2013/acpd-13-17953-2013-supplement.pdf.

Acknowledgements. The authors would like to thank the Wyoming Department of Environmental Quality (WDEQ) for their support. Support by MSI, especially by Bill Hauze and Tyler Ward is greatly appreciated.

References

Bader, D. C. and McKee, T. B.: Effects of shear, stability and valley characteristics on the destruction of temperature inversions, J. Clim. Appl. Meteorol., 24, 822–832, 1985.

Bejan, I., Abd El Aal, Y., Barnes, I., Benter, T., Bohn, B., Wiesen, P., and Kleffmann, J.: The photolysis of ortho-nitrophenols: an new gas phase source of HONO, Phys. Chem. Chem. Phys. 8, 2028–2035, 2006.

Björkman, M. P., Kühnel, R., Partridge, D. G., Roberts, T. J., Aas, W., Mazzola, M., Viola, A., Hodson, A., Ström, J., and Isaksson, E.: Nitrate dry deposition in Svalbord, Tellus B, 65, 1–18, doi:10.3402/tellusb.v65i0.19071, 2013.

Carter, W. P. L. and Seinfeld, J. H.: Winter ozone formation and VOC incremental reactivities in the Upper Green River Basin of Wyoming, Atmos. Environ., 50, 255–266, doi:10.1016/j.atmosenv.2011.12.025, 2012.

Chameides, W. L., Fehsenfeld, F., Rodgers, M. O., Cardelino, C., Martinez, J., Parrish, D., Lonneman, W., Lawson, D. R., Rasmussen, R. A., Zimmerman, P., Greenberg, J., Middleton, P., and Wang, T.: Ozone precursor relationships in the ambient air, J. Geophys. Res., 97, 6037–6055, 1992.

Czader, B. H., Li, X., and Rappenglueck, B.: CMAQ modeling and analysis of radicals, radical precursors and chemical transformations, J. Geophys. Res., in revision, 2013.

ACPD
13, 17953–18005, 2013

Czader, B. H., Rappenglück, B., Percell, P., Byun, D. W., Ngan, F., and Kim, S.: Modeling nitrous acid and its impact on ozone and hydroxyl radical during the Texas Air Quality Study 2006, Atmos. Chem. Phys., 12, 6939–6951, doi:10.5194/acp-12-6939-2012, 2012.

Draxler, R. R. and Rolph, G. D.: HYSPLIT (HYbrid Single-Particle Lagrangian Integrated Trajectory) Model access via NOAA ARL READY Website, available at: http://ready.arl.noaa.gov/HYSPLIT.php (last access: March 2013), NOAA Air Resources Laboratory, Silver Spring, MD, 2013.

Edwards, P. M., Young, C. J., Aikin, K., deGouw, J. A., Dubé, W. P., Geiger, F., Gilman, J. B., Helmig, D., Holloway, J. S., Kercher, J., Lerner, B., Martin, R., McLaren, R., Parrish, D. D., Peischl, J., Roberts, J. M., Ryerson, T. B., Thornton, J., Warneke, C., Williams, E. J., and Brown, S. S.: Ozone photochemistry in an oil and natural gas extraction region during winter: simulations of a snow-free season in the Uintah Basin, Utah, Atmos. Chem. Phys. Discuss., 13, 7503–7552, doi:10.5194/acpd-13-7503-2013, 2013.

EIA (US Energy Information Administration): Top 100 Oil and Gas Fields, available at: http://www.eia.gov/oil_gas/rpd/topfields.pdf, accessed February 2013, 2009.

Elshorbany, Y. F., Kurtenbach, R., Wiesen, P., Lissi, E., Rubio, M., Villena, G., Gramsch, E., Rickard, A. R., Pilling, M. J., and Kleffmann, J.: Oxidation capacity of the city air of Santiago, Chile, Atmos. Chem. Phys., 9, 2257–2273, doi:10.5194/acp-9-2257-2009, 2009.

Field, R. A., Soltis, J., and Montague, D.: Pinedale Anticline Spatial Air Quality Assessment (PASQUA), Mobile laboratory monitoring of ozone precursors, Boulder South Road site 10/29/2010 to 05/02/2011, Summary Report, University of Wyoming, Laramie, Wyoming, available at: http://www-das.uwyo.edu/ozone/index.html (last access: February 2013), 2011.

Field, R. A., Soltis, J., and Montague, D.: Pinedale Anticline Spatial Air Quality Assessment (PASQUA), 2011–2012 Spatial Distribution Surveys, Summary Report, University of Wyoming, Laramie, Wyoming, available at: http://www-das.uwyo.edu/ozone/index.html (last access: February 2013), 2012a.

Field, R. A., Soltis, J., and Montague, D.: Temporal and Spatial Distributions of Volatile Organic Compounds Associated with Oil and Gas Development in the Upper Green River Basin of Wyoming, Invited in Session: A21J American Geophysical Union, Fall Meeting, San Francisco, CA, USA, 3–7 December 2012, 2012b.

Finlayson-Pitts, B. J. and Pitts Jr., J. N.: Chemistry of the Upper and Lower Atmosphere, Academic Press, San Diego, 969 pp., 2000.

ACPD
13, 17953–18005, 2013

Finlayson-Pitts, B. J., Wingen, L. M., Sumner, A. L., Syomin, D., and Ramazan, K. A.: The heterogeneous hydrolysis of NO_2 in laboratory systems and in outdoor and indoor atmospheres: an integrated mechanism, Phys. Chem. Chem. Phys., 5, 223–242, 2003.

Goodman, A. L., Underwood, G. M., and Grassian, V. H.: Heterogeneous reaction of NO_2: characterization of gas-phase and adsorbed products from the reaction, $2\,NO_2(g)+H_2O(a) \rightarrow HONO(g)+HNO_3(a)$ on hydrated silica particles, J. Phys. Chem. A, 103, 7217–7223, 1999.

Hauglstaine, D. A., Granier, C., Brasseur, G. P., and Megie, G.: The importance of atmospheric chemistry inthe calculation of radiative forcing on the climate system, J. Geophys. Res., 99,1173–1186, 1994.

Hayden, K. L., Anlauf, K. G., Hastie, D. R., and Bottenheim, J. W.: Partitioning of reactive atmospheric nitrogen oxides at an elevated site in southern Quebec, Canada, J. Geophys. Res., 108, 4603, doi:10.1029/2002JD003188, 2003.

Heland, J., Kleffmann, J., Kurtenbach, R., and Wiesen, P.: A new instrument to measure gaseous nitrous acid (HONO) in the atmosphere, Environ. Sci. Technol., 35, 3207–3212, 2001.

Helmig, D., Cohen, L. D., Bocquet, F., Oltmans, S., Grachev, A., and Neff, W.: Spring and summertime diurnal surface ozone fluxes over the polar snow at Summit, Greenland, Geophys. Res. Lett., 36, L08809, doi:10.1029/2008GL036549, 2009.

Jacobson, M. Z.: Air Pollution and Global Warming, History, Science, and Solutions, Cambridge University Press, 406 pp., New York/USA, 2012.

Jenkin, M. I., Cox, R. A., and Williams, D. J.: Laboratory studies of the kinetics of formation of nitrous acid from the thermal reaction of nitrogen dioxide and water vapour, Atmos. Environ., 22, 487–498, 1988.

Kirchstetter, T. W., Harley, R. A., and Littlejohn, D.: Measurement of nitrous acid in motor vehicle exhaust, Environ. Sci. Technol., 30, 2843–2849, 1996.

Kleffmann, J.: Daytime sources of nitrous acid (HONO) in the atmospheric boundary layer, Chem. Phys., 8, 1137–1144, 2007.

Kleffmann, J., Becker, K. H., and Wiesen, P.,: Heterogeneous NO_2 conversion processes on acid surfaces: possible atmospheric implications, Atmos. Environ., 32, 2721–2729, 1998.

Kleffmann, J., Heland, J., Kurtenbach, R., Lörzer, J. C., and Wiesen, P.: A new instrument (LOPAP) for the detection of nitrous acid (HONO), Environ. Sci. Pollut. Res., 9, 48–54, 2002.

Lefer, B. and Rappenglück, B.: The TexAQS-II radical and aerosol measurement project (TRAMP), Atmos. Environ., 44, 3997–4004, doi:10.1016/j.atmosenv.2010.05.053, 2010.

ACPD
13, 17953–18005, 2013

Leuchner, M. and Rappenglück, B.: VOC Source-Receptor Relationships in Houston during TexAQS-II, Atmos. Environ., 44, 4056–4067, doi:10.1016/j.atmosenv.2009.02.029, 2010.
Li, S. P., Matthews, J., and Sinha, A.: Atmospheric hydroxyl radical production from electronically excited NO_2 and H_2O, Science, 319, 1657–1660, 2008.
Luke, W. T., Kelley, P., Lefer, B. L., Flynn, J., Rappenglück, B., Leuchner, M., Dibb, J. E., Ziemba, L. D., Anderson, C. H., and Buhr, M.: Measurements of primary trace gases and NO_y composition in Houston, Texas, Atmos. Environ., 44, 4068–4080, doi:10.1016/j.atmosenv.2009.08.014, 2010.
Mack, J. and Bolton, J. R.: Photochemistry of nitrite and nitrate in aqueous solution: a review, J. Photochem. Photobiol. A, 128, 1–13, 1999.
Mao, J., Ren, X., Chen, S., Brune, W. H., Chen, Z., Martinez, M., Harder, H., Lefer, B., Rappenglück, B., Flynn, J., and Leuchner, M.: Atmospheric oxidation capacity in the summer of Houston 2006: comparison with summer measurements in other metropolitan studies, Atmos. Environ., 44, 4107–4115, doi:10.1016/j.atmosenv.2009.01.013, 2010.
McLaren, R., Salmon, R. A., Liggio, J., Hayden, K. L., Anlauf, K. G., and Leaitch, W. R., Nighttime chemistry at a rural site in the Lower Fraser Valley, Atmos. Environ., 38, 5837–5848, 2004.
MSI (Meteorological Solutions Inc.): Final Report – 2009 Upper Green River Ozone Study, Report to Wyoming Department of Environmental Quality (WDEQ), Cheyenne, WY, October 2009, 2009.
MSI (Meteorological Solutions Inc.): Final Report 2011 Upper Green River Ozone Study, Report to Wyoming Department of Environmental Quality (WDEQ), Cheyenne, WY, October 2011, 2011.
Olaguer, E. P., Kolb, C. E., Lefer, B., Rappenglück, B., Zhang, R., and Pinto, J. P.: Overview of the SHARP campaign: motivation, design, and major outcomes, J. Geophys. Res., accepted, 2013.
Parrish, D. D., Allen, D. T., Bates, T. S., Estes, M., Fehsenfeld, F. C., Feingold, G., Ferrare, R., Hardesty, R. M., Meagher, J. F., Nielsen-Gammon, J. W., Pierce, R. B., Ryerson, T. B., Seinfeld, J. H., and Williams, E. J.: Overview of the second Texas air quality study (TexAQS-II) and the Gulf of Mexico atmospheric composition and climate study (GoMACCS), J. Geophys. Res., 114, D00F13, doi:10.1029/2009JD011842, 2009.
Ramazan, K. A., Wingen, L. M., Miller, Y., Chaban, G. M., Gerber, R. B., Xantheas, S. S., and Finlayson-Pitts, B. J.: New experimental and theoretical approach to the heterogeneous

ACPD
13, 17953–18005, 2013

hydrolysis of NO_2: key role of molecular nitric acid and its complexes, J. Phys. Chem. A, 110, 6886–6897, 2006.
Rappenglück, B.: WDEQ UGWOS 2010 HONO Measurements, Report to Meteorological Solutions Inc., Salt Lake City, UT, May 2010, 2010.
Rappenglück, B.: WDEQ UGWOS 2011 HONO Measurements, Report to Meteorological Solutions Inc., Salt Lake City, UT, August 2011, 2011.
Rappenglück, B., Dasgupta, P. K., Leuchner, M., Li, Q., and Luke, W.: Formaldehyde and its relation to CO, PAN, and SO_2 in the Houston-Galveston airshed, Atmos. Chem. Phys., 10, 2413–2424, doi:10.5194/acp-10-2413-2010, 2010.
Rappenglück, B., Lubertino, G., Alvarez, S., Golovko, J., Czader, B., and Ackermann, L.: Radical precursors and related species from traffic as observed and modeled at an urban highway junction, J. Air Waste Manag. Assoc., accepted, 2013.
Reidmiller, D. R., Jaffe, D. A., Fischer, E. V., and Finley, B.: Nitrogen oxides in the boundary layer and free troposphere at the Mt. Bachelor Observatory, Atmos. Chem. Phys., 10, 6043–6062, doi:10.5194/acp-10-6043-2010, 2010.
Ren, X., van Duin, D., Cazorla, M., Chen, S., Mao, J., Brune, W. H., Flynn, J. H., Grossberg, N., Lefer, B. L., Rappenglück, B., Wong, K. W., Tsai, C., Stutz, J., Dibb, J. E., Jobson, B. T., Luke, W. T., and Kelley, P.: Atmospheric oxidation chemistry and ozone production: results from SHARP 2009 in Houston, Texas, J. Geophys. Res., in press, 2013.
Ridley, B. A., Shetter, J. D., Gandrug, B. W., Salas, L. J., Singh, H. B., Caroll, M. A., Hübler, G., Albritton, D. L., Hastie, D. R., Schiff, H. I., Mackay, G. I., Karechi, D. R., Davies, D. D., Bradshaw, J. D., Rodgers, M. O., Sandholm, S. T., Torres, A. L., Condon, E. P., Gregory, G. L., and Beck, S. M.: Ratios of peroxyacetylnitrate to active nitrogen observed during aircraft flights over the eastern Pacific oceans and continental United States, J. Geophys. Res., 95, 10179–10192, 1990.
Ródenas, M., Muñoz, A., Alacreu, F., Dorn, H.-P., Brauers, T., Kleffmann, J., Mikuška, P., Večeřa, Z., Häseler, R., Ye, C., Ruth, A., Dixneuf, S., Venables, D., Darby, S., Chen, J., Ashu-ayem, E., Elshorbany, Y., Voigt, C., Jessberger, P., Kaufmann, S., Schäuble, D., Mellouki, A., Cazaunau, M., Grosselin, B., Colomb, A., Michoud, V., Miet, K., Ball, S., Daniels, M., Goodall, I., Tan, D., Stickel, R., Case, A., Rappenglück, B., Croxatto, G., Percival, C., Bacak, A., Mcguillen, M., Dibb, J., Scheuer, E., Zhou, X., Ferm, M., Varma, R., Pilling, M., Clemente, E., Porras, R., Vera, T., Vázquez, M., Borrás, E., Valero, J., and Bloss, W.: The

ACPD
13, 17953–18005, 2013

FIONA campaign (EUPHORE): Formal Intercomparison of Observations of Nitrous Acid, EGU Joint Assembly, Vienna/Austria, 3–9 April 2011, 2011.
Rolph, G. D.: Real-time Environmental Applications and Display sYstem (READY) Website (http://ready.arl.noaa.gov), NOAA Air Resources Laboratory, Silver Spring, MD, 2013.
Schnell, R. C., Oltmans, S. J., Neely, R. R., Endres, M. S., and Molenar, J. V.,: Rapid photochemical production of ozone at high concentrations in a rural site during winter, Nat. Geosci., 2, 120–123, 2009.
Sillman, S.: Observation-based methods (OBMs) for analyzing urban/regional ozone production and Ozone-NO_x-VOC sensitivity, Report to EPA, 1-D-57-95-NTEX, available at: http://www-personal.umich.edu/~sillman/obm.htm, accessed 2013, 2002.
Sillman, S. and He, D.: Some theoretical results concerning O_3-NO_x-VOC chemistry and NO_x-VOC indicators, J. Geophys. Res., 107, 4659, doi:10.1029/2001JD001123, 2002.
Sommariva, R., Trainer, M., de Gouw, J. A., Roberts, J. M., Warneke, C., Atlas, E., Flocke, F., Goldan, P. D., Kuster, W. C., Swanson, A. L., and Fehsenfeld, F. C.: A study of organic nitrates formation in an urban plume using a Master Chemical Mechanism, Atmos. Environ., 42, 5771–5786, 2008.
Stemmler, K., Ndour, M., Elshorbany, Y., Kleffmann, J., D'Anna, B., George, C., Bohn, B., and Ammann, M.: Light induced conversion of nitrogen dioxide into nitrous acid on submicron humic acid aerosol, Atmos. Chem. Phys., 7, 4237–4248, doi:10.5194/acp-7-4237-2007, 2007.
Stull, R. B.: An Introduction to Bounday Layer Meteorology, Springer, 684 pp., Dordrecht/The Netherlands, 1988.
Stutz, J., Alicke, B., Ackermann, R., Geyer, A., Wang, S., White, A. B., Williams, E. J., Spicer, E. J., and Fast, J. D.: Relative humidity dependence of HONO chemistry in urban areas, J. Geophys. Res., 109, D03307, doi:10.1029/2003JD004135, 2004.
Stutz, J., Oh, H.-J., Whitlow, S. I., Anderson, C. H., Dibb, J. E., Flynn, J., Rappenglück, B., and Lefer, B.: Simultaneous DOAS and Mist-Chamber IC measurements of HONO in Houston, TX, Atmos. Environ., 44, 4090–4098, doi:10.1016/j.atmosenv.2009.02.003, 2010a.
Stutz, J., Wong, K. W., Lawrence, L., Ziemba, L., Flynn, J. H., Rappenglück, B., and Lefer, B.: Nocturnal NO_3 radical chemistry in Houston, TX, Atmos. Environ., 44, 4099–4106, doi:10.1016/j.atmosenv.2009.03.004, 2010b.
US EPA (US Environmental Protection Agency: Area Designations for 2008 Ground-level Ozone Standards, available at: http://www.epa.gov/ozonedesignations/2008standards/final/region8f.htm, last access: February 2013), 2012.

ACPD
13, 17953–18005, 2013

Villena, G., Wiesen, P., Cantrell, C. A., Flocke, F., Fried, A., Hall, S. R., Hornbrook, R. S., Knapp, D., Kosciuch, E., Mauldin III, R. L., McGrath, J. A., Montzka, D., Richter, D., Ullmann, K., Walega, J., Weibring, P., Weinheimer, A., Staebler, R. M., Liao, J., Huey, L. G., and Kleffman, J.: Nitrous acid (HONO) during polar spring in Barrow, Alaska: a net source of OH radicals?, J. Geophys. Res., 116, D00R07, doi:10.1029/2011JD016643, 2011.

WDEQ: 2011 Winter Upper Green River Basin Emission Inventory, Wyoming Department of Environmental Quality (WDEQ), Cheyenne, Wyoming, 2011.

Wojtal, P., Halla, J. D., and McLaren, R.: Pseudo steady states of HONO measured in the nocturnal marine boundary layer: a conceptual model for HONO formation on aqueous surfaces, Atmos. Chem. Phys., 11, 3243–3261, doi:10.5194/acp-11-3243-2011, 2011.

Yu, C.-H. and Pielke, R. A.: Mesoscale air quality under stagnant synoptic cold season conditions in the Lake Powell area, Atmos. Environ., 20, 1751–1762, 1986.

Zhou, X., Beine, H. J., Honrath, R. E., Fuentes, J. D., Simpson, W., Shepson, P. B., and Bottenheim, J. W.: Snowpack photochemical production of HONO: a major source of OH in the arctic boundary layer in springtime, Geophys. Res. Lett., 28, 4087–4090, 2001.

Zhou, X., Gao, H., He, Y., and Huang, G.: Nitric acid photolysis on surfaces in low-NO_x environments: significant atmospheric implications, Geophys. Res. Lett., 2217, 30, doi:10.1029/2003GL018620, 2003.

Zhou, X. L., He, Y., Huang, G., Thornberry, T. D., Carroll, M. A., and Bertman, S. B.,: Photochemical production of nitrous acid on glass sample manifold surface, Geophys. Res. Lett., 29, 1681, doi:10.1029/2002GL015080, 2002.

Ziemba, L. D., Dibb, J. E., Griffin, R. J., Anderson, C. H., Whitlow, S. L., Lefer, B. L., Rappenglück, B., and Flynn, J.: Heterogeneous conversion of nitric acid to nitrous acid on the surface of primary organic aerosol in an urban atmosphere, Atmos. Environ., 44, 4081–4089, doi:10.1016/j.atmosenv.2008.12.024, 2010.

ACPD
13, 17953–18005, 2013

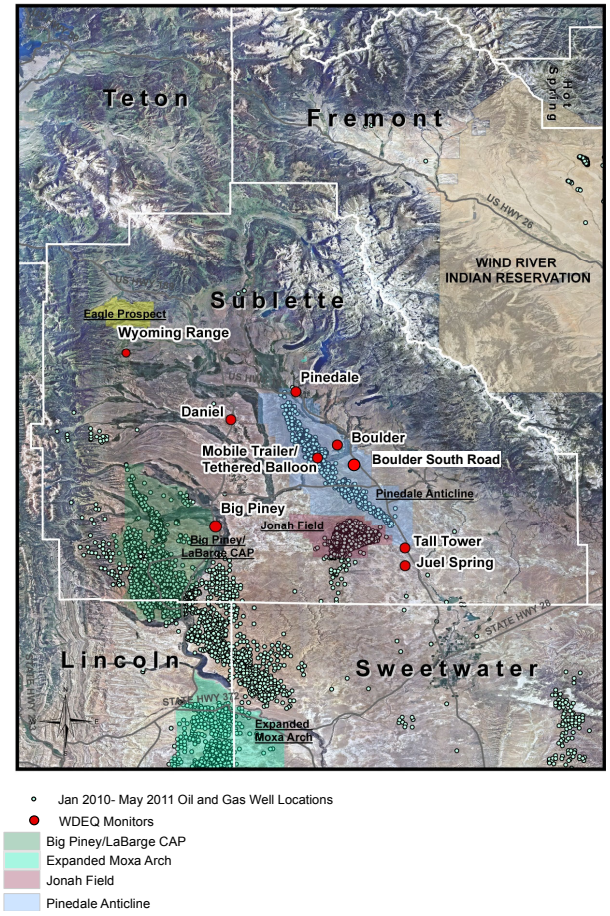

Fig. 1. The monitoring sites "Boulder", "Boulder South Road", "Tethered Balloon" and other WDEQ (Wyoming Department of Environmental Quality) monitoring sites relative to the locations of oil and gas well locations operating during January–March 2011.

ACPD
13, 17953–18005, 2013

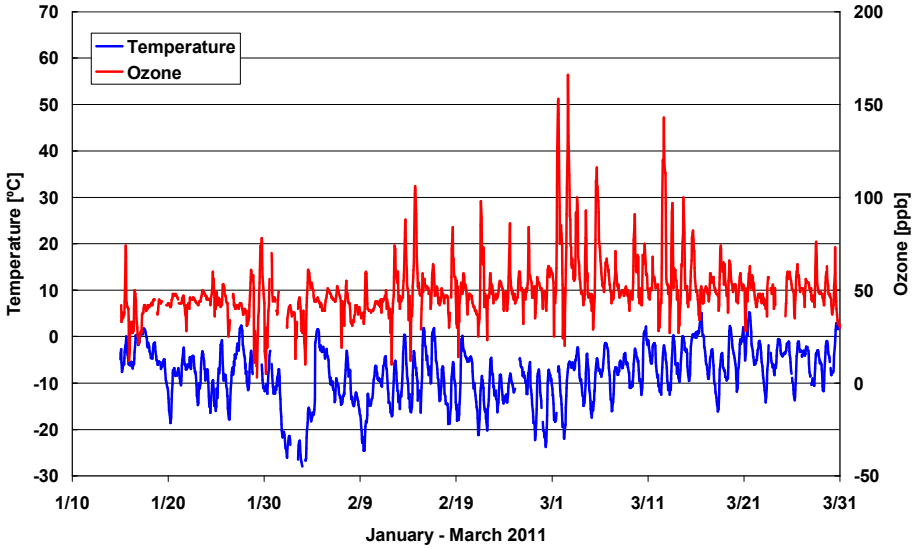

Fig. 2. Time series for ozone and temperature based on hourly data at the Boulder site for January–March 2011.

ACPD
13, 17953–18005, 2013

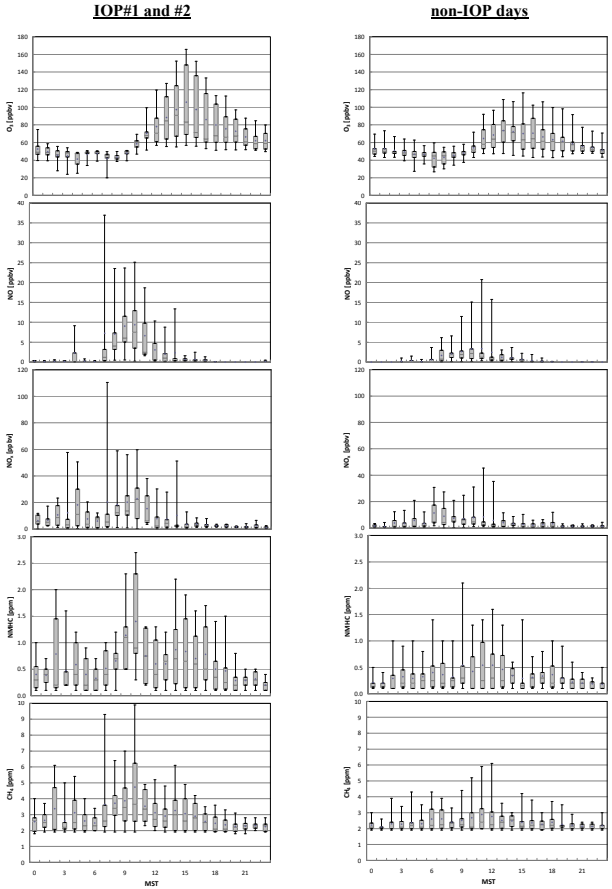

Fig. 3a. Mean diurnal variation of selected trace gases for IOP and non-IOP days.

ACPD
13, 17953–18005, 2013

Strong wintertime ozone events in Wyoming

B. Rappenglück et al.

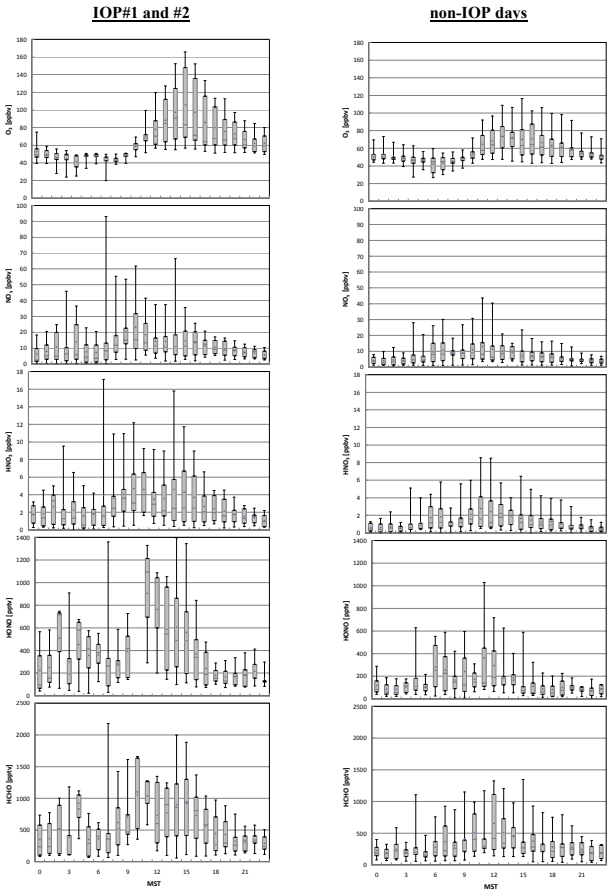

Fig. 3b. Mean diurnal variation of selected trace gases for IOP and non-IOP days.

ACPD
13, 17953–18005, 2013

Strong wintertime ozone events in Wyoming

B. Rappenglück et al.

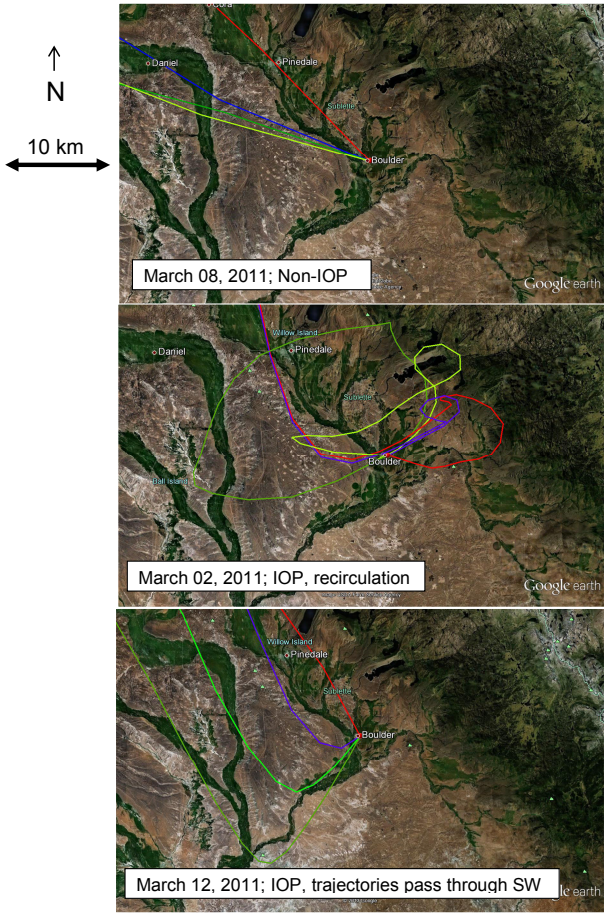

Fig. 4. HYSPLIT backward trajectories calculated for 50 m a.g.l. and for following arrival times at Boulder: 07:00 MST (red), 12:00 MST (blue), 14:00 MST (light green), and 17:00 MST (dark green).

ACPD
13, 17953–18005, 2013

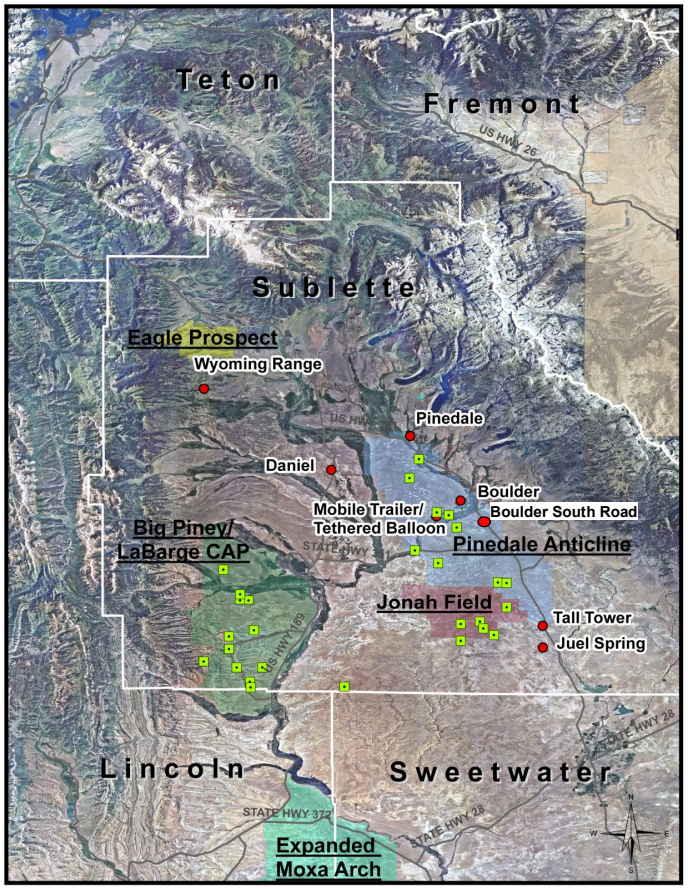

Fig. 5. Locations of compressors (green rectangles) operating during January–March 2011 relative to the Boulder monitoring site.

ACPD
13, 17953–18005, 2013

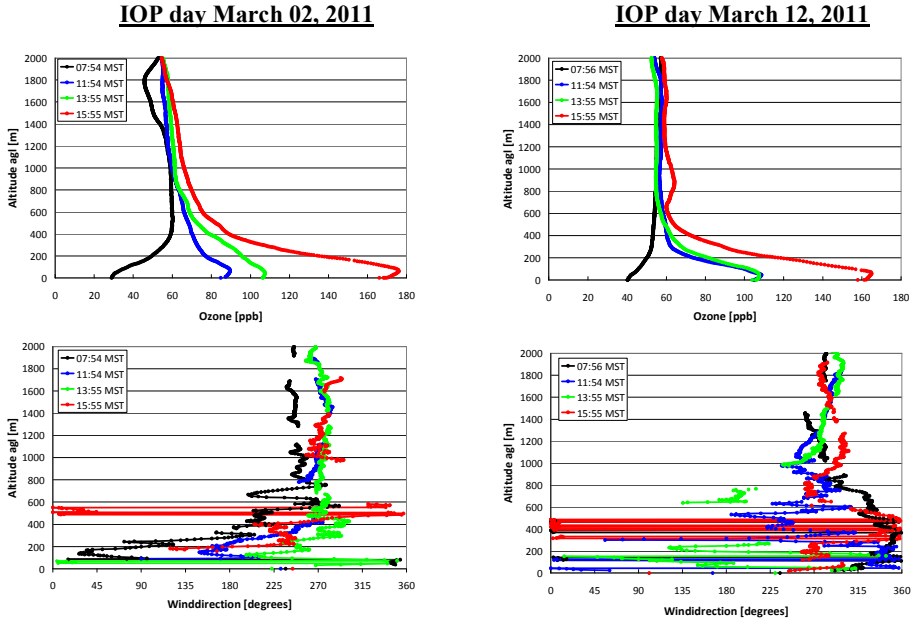

Fig. 6. Profiles of ozone (above) and wind direction (below) on IOP days 2 March 2011 (left) and 12 March 2011 (right).

ACPD
13, 17953–18005, 2013

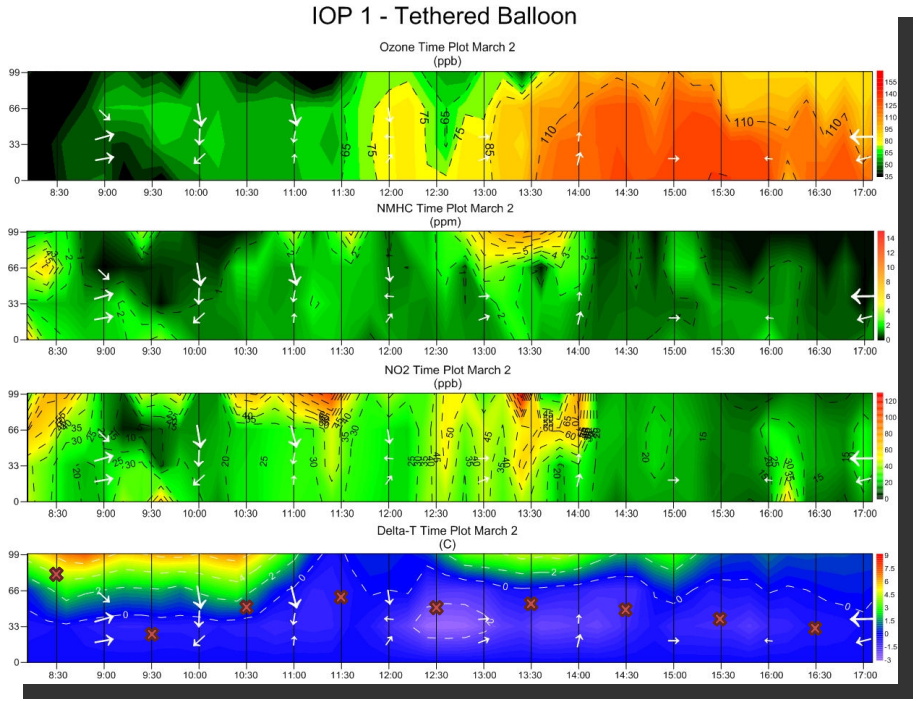

Fig. 7. Results from tethersonde measurements of ozone, NMHC, NO_2, and ΔT (Delta-T) on 2 March 2011. ΔT is defined as the temperature at a given level minus the temperature at the surface. Mixing layer heights as determined by SODAR data are indicated as "x" in the ΔT plot.

ACPD
13, 17953–18005, 2013

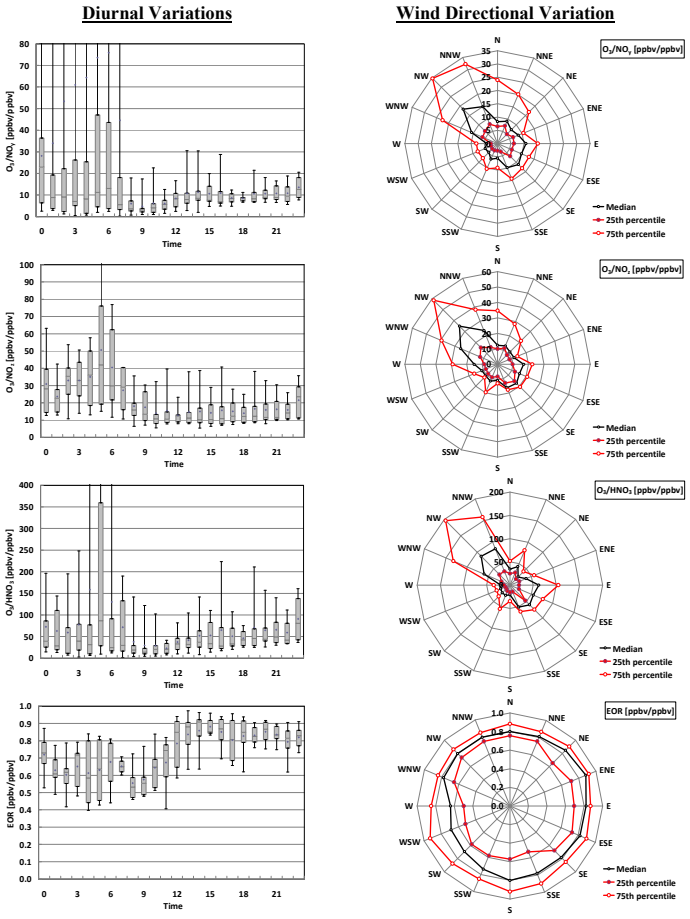

Fig. 8. Diurnal and wind directional variation of photochemical indicators O_3/NO_y, O_3/NO_z, O_3/HNO_3 and EOR on IOP days. Units shown in brackets for the wind directional variation plots refer to the radial direction of the corresponding trace gas plot.

ACPD
13, 17953–18005, 2013

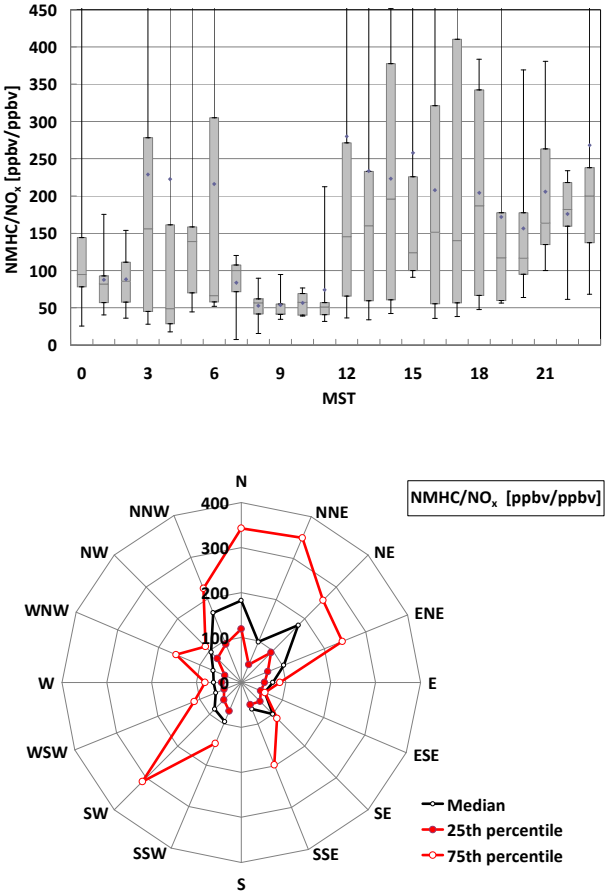

Fig. 9. Diurnal and wind directional variation of the NMHC/NO_x ratio at the Boulder site on IOP days. Units shown in brackets for the wind directional variation plots refer to the radial direction of the corresponding trace gas plot.

ACPD
13, 17953–18005, 2013

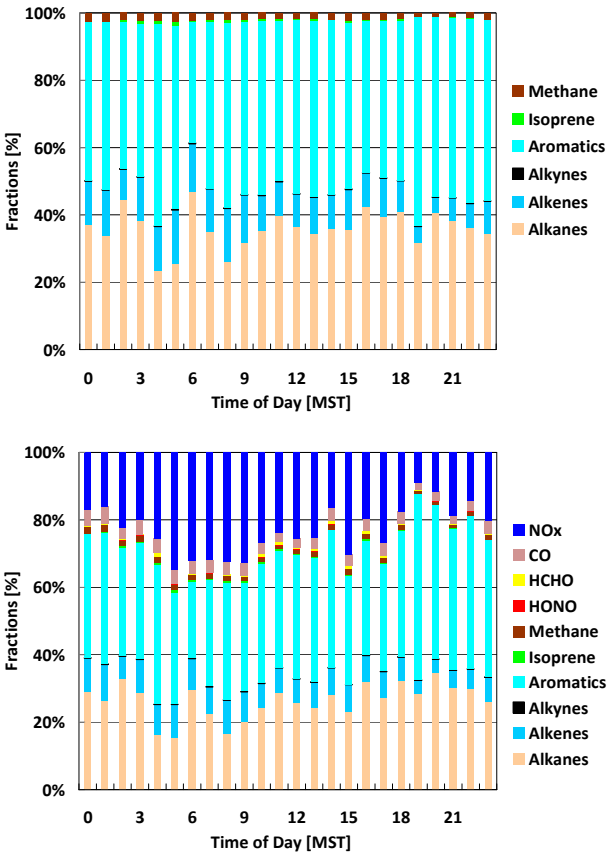

Fig. 10. Diurnal variation of fractions of propene-equivalent on IOP days. Above: NMHC classes and CH_4 only. Below: same as above, but in addition NO_x, CO, HCHO, and HONO. Speciated NMHC, NO_x, and CO data from the Boulder South Road site.

ACPD
13, 17953–18005, 2013

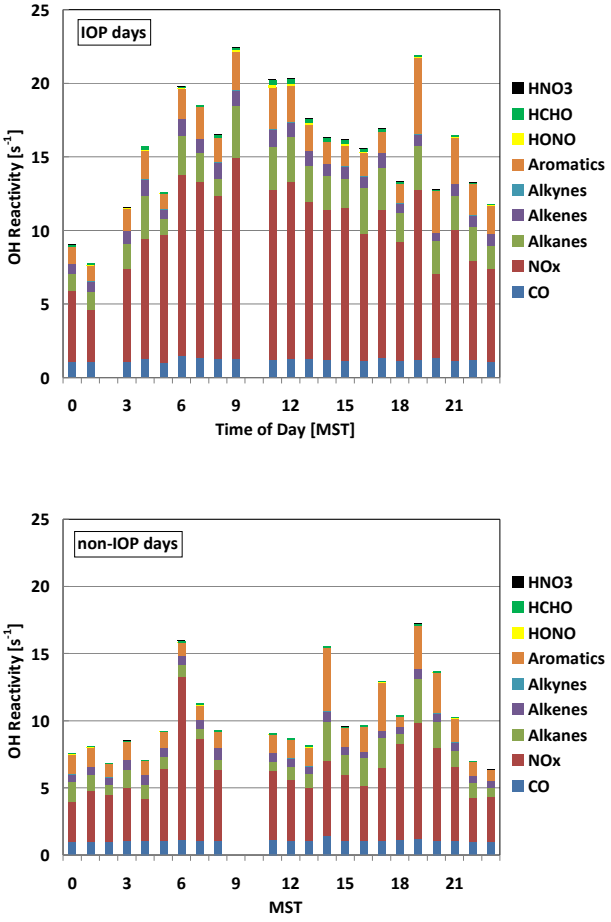

Fig. 11. OH reactivity on IOP days (above) and non-IOP days (below). Speciated NMHC, NO_x, and CO data from the Boulder South Road site.

ACPD
13, 17953–18005, 2013

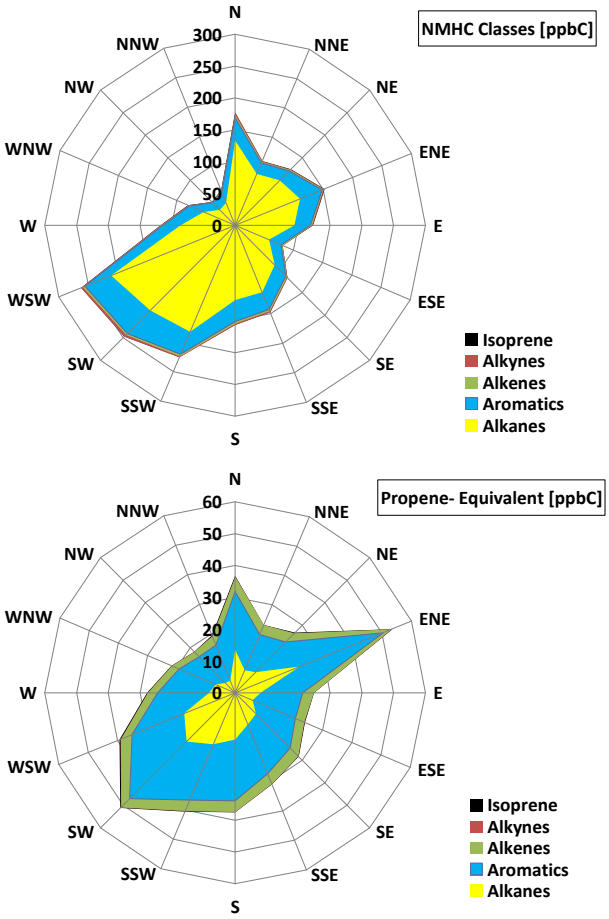

Fig. 12. Wind directional dependence of NMHC classes and the propene equivalent for all days. Speciated NMHC data from the Boulder South Road site. Units shown in brackets refer to the radial direction of the corresponding trace gas plot.

ACPD
13, 17953–18005, 2013

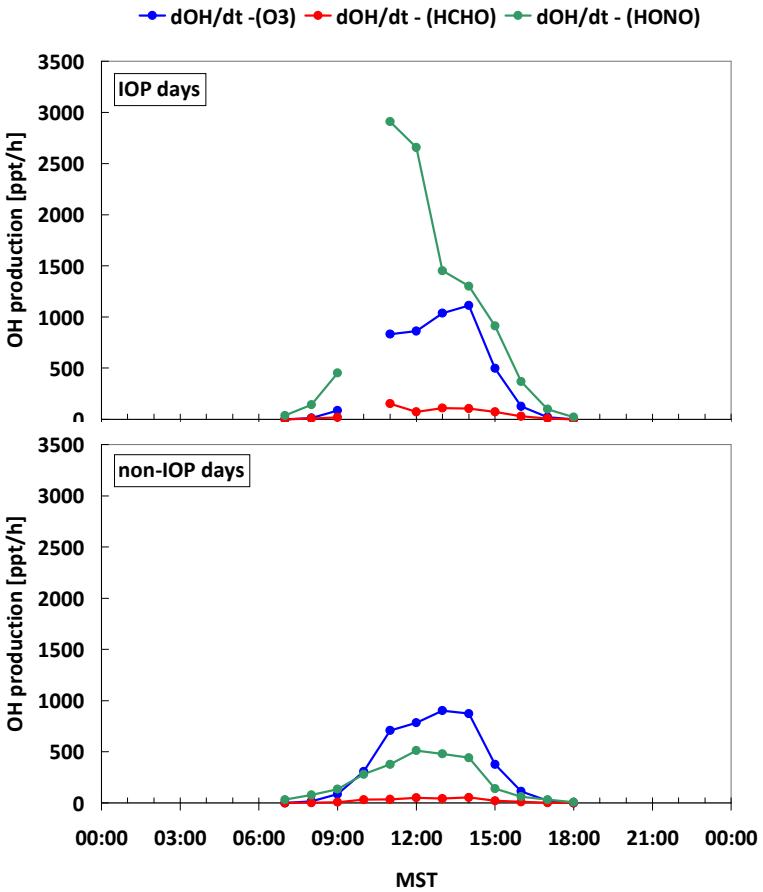

Fig. 13. OH production due to photolysis of ozone, HCHO, and HONO for IOP and non-IOP days. Photolysis rates were calculated based on latitude 43° N, date 1 March, 80 % albedo, and cloudless conditions using approaches in Finlayson-Pitts and Pitts (2000) and references therein.

ACPD
13, 17953–18005, 2013

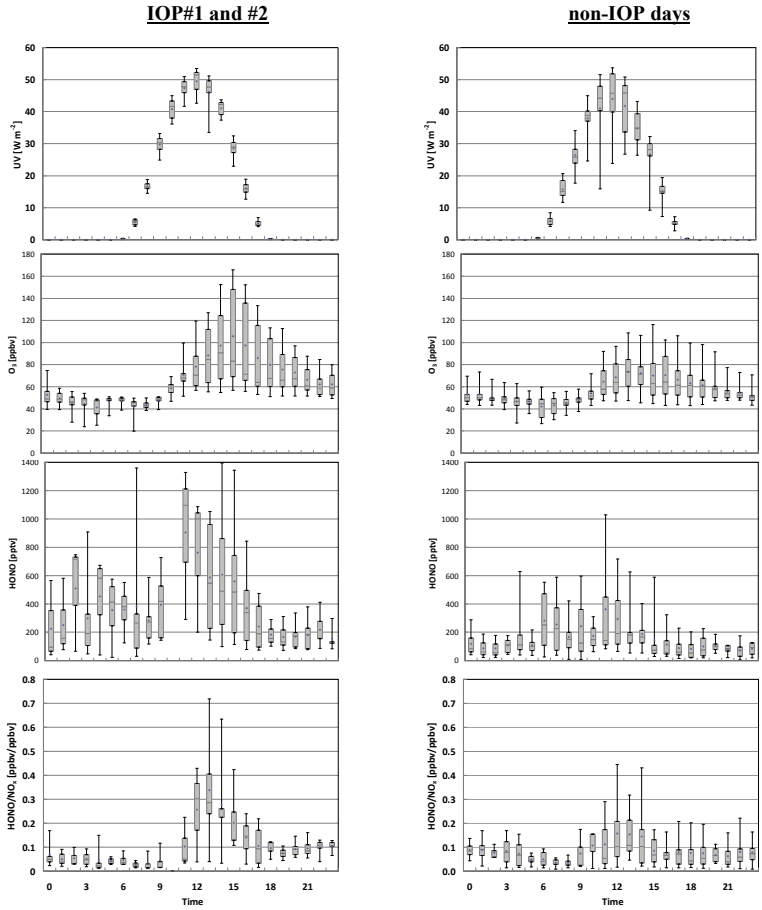

Fig. 14. Mean diurnal variation of incoming UV radiation, ozone, HONO, and the HONO/NO_x ratio for IOP and non-IOP days.

ACPD
13, 17953–18005, 2013